AD-A086 871 TEXAS UNIV AT AUSTIN APPLIED RESEARCH LABS F/G 20/1
INVESTIGATION OF A PHASE-LOCKED LOOP RECEIVER FOR A PARAMETRIC --ETC(U)
MAY 80 R A LAMB N00024-77-C-6200
UNCLASSIFIED ARL-TR-80-25 NL

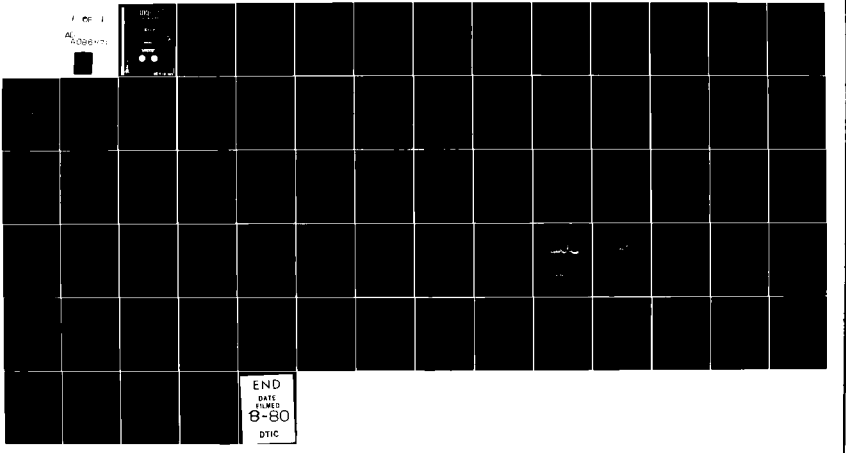

END
DATE FILMED
8-80
DTIC

AD A086871

UNCLASSIFIED

SECURITY CLASSIFICATION OF THIS PAGE (When Data Entered)

REPORT DOCUMENTATION PAGE	READ INSTRUCTIONS BEFORE COMPLETING FORM
1. REPORT NUMBER / 2. GOVT ACCESSION NO. AD-A086 871	3. RECIPIENT'S CATALOG NUMBER
4. TITLE (and Subtitle) INVESTIGATION OF A PHASE-LOCKED LOOP RECEIVER FOR A PARAMETRIC ACOUSTIC RECEIVING ARRAY	5. TYPE OF REPORT & PERIOD COVERED Technical Report
	6. PERFORMING ORG. REPORT NUMBER ARL-TR-80-25
7. AUTHOR(s) Robert A. Lamb	8. CONTRACT OR GRANT NUMBER(s) N00024-77-C-6200
9. PERFORMING ORGANIZATION NAME AND ADDRESS Applied Research Laboratories The University of Texas at Austin Austin, Texas 78712	10. PROGRAM ELEMENT, PROJECT, TASK AREA & WORK UNIT NUMBERS Item 0011
11. CONTROLLING OFFICE NAME AND ADDRESS Naval Sea Systems Command Department of the Navy Washington DC 20362	12. REPORT DATE 5 May 1980
	13. NUMBER OF PAGES
14. MONITORING AGENCY NAME & ADDRESS (if different from Controlling Office)	15. SECURITY CLASS. (of this report) Unclassified
	15a. DECLASSIFICATION DOWNGRADING SCHEDULE NA

16. DISTRIBUTION STATEMENT (of this Report)

Approved for public release; distribution unlimited.

17. DISTRIBUTION STATEMENT (of the abstract entered in Block 20, if different from Report)

18. SUPPLEMENTARY NOTES

19. KEY WORDS (Continue on reverse side if necessary and identify by block number)

PARRAY
Nonlinear Acoustics
Parametric Reception
Phase-Locked Loop Demodulation

20. ABSTRACT (Continue on reverse side if necessary and identify by block number)

This report describes the investigation of a phase-locked loop (PLL) demodulator considered for use with the parametric acoustic receiving array (PARRAY). The PARRAY as an acoustic sensor is explained and the effects of longitudinal transducer motion on the PARRAY are described. This transducer vibration produces intermodulation products between the desired acoustic signals and the vibration induced signals. Both theoretical analysis and experimental data showing that the PLL demodulator can reduce this intermodulation

DD FORM 1 JAN 73 1473 EDITION OF 1 NOV 65 IS OBSOLETE

UNCLASSIFIED 404 134

SECURITY CLASSIFICATION OF THIS PAGE (When Data Entered)

20. (Cont'd)

in a PARRAY are given. Comparison is made between theoretically predicted PLL intermodulation reduction and measurements taken with simulated PARRAY signals. Also, experimental data are described showing the operation of the demodulator with a PARRAY undergoing transducer vibration.

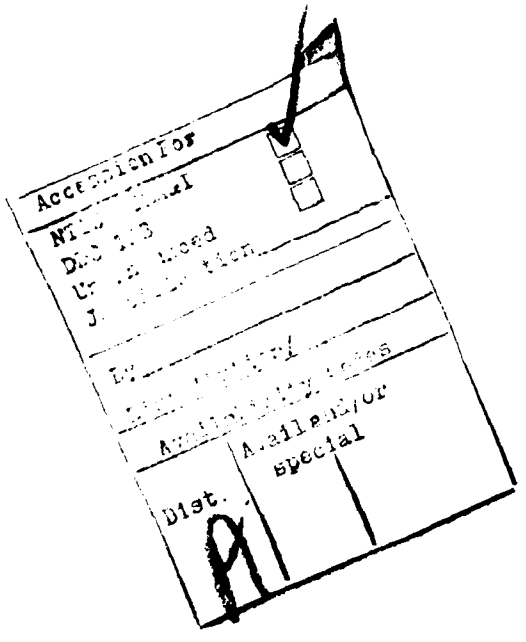

TABLE OF CONTENTS

LIST OF FIGURES

CHAPTER I

INTRODUCTION

The subject of this report is application of a phase-locked loop (PLL) demodulator to the parametric acoustic receiving array (PARRAY). The use of a PLL demodulator in processing PARRAY signals is studied both theoretically and experimentally. Measurements made in this investigation confirm that the PLL demodulator is useful in reducing undesirable effects due to vibration of PARRAY transducers. In this chapter the PARRAY will be briefly introduced in order to define the problem under investigation, and an overview of the investigation will be given.

The PARRAY presents a difficult signal processing problem. Basically, the PARRAY is a directional acoustic receiver that exploits the nonlinearity of the medium. When a carrier wave is injected into the medium, this nonlinearity produces phase modulation of the carrier by acoustic signals present in the medium. Demodulation of the signal received some distance from the carrier source provides directional acoustic reception. Because of the very weak nonlinearity of water, wide dynamic range receivers must be used to detect the modulation produced.

Longitudinal transducer vibration produces phase modulation of the PARRAY sideband signals. Low frequency transducer vibration may significantly degrade performance of a PARRAY, especially in mobile applications. The PLL demodulator seems ideally suited to reduce the effects of transducer vibration by tracking the low frequency vibration induced carrier phase variations. It is the purpose of this report to analyze and

describe the application of the PLL receiver to the PARRAY signal processing problem.

Chapter II outlines the basic principles of PARRAY operation, and discusses the sensitivity of the PARRAY to transducer vibration. The chapter also summarizes linear PLL theory, and presents a derivation of the operation of a narrowband PLL demodulator with an input much like the PARRAY output signal.

The experimental investigation of a PLL demodulator is described in Chapter III. Measurements of the noise, frequency response, and intermodulation performance of the PLL receiver are described and compared to theory. Performance of the PLL receiver with a PARRAY undergoing transducer vibration is also described. These tests, especially the PARRAY vibration test, show that the PLL receiver is useful in situations where high level low frequency transducer vibrations are present.

A summary and discussion of results are presented in Chapter IV.

CHAPTER II

THEORETICAL CONSIDERATIONS

The purpose of this chapter is to describe PARRAY operation and the effects of transducer motion on a PARRAY, and to develop theoretical predictions for the performance of a phase-locked loop demodulator in reducing the effects of transducer motion.

A. PARRAY Operation and Effects of Transducer Vibration

1. PARRAY Operation

The PARRAY employs two high frequency transducers and associated electronic equipment and exploits the slight nonlinearity of water to achieve directional reception of low frequency acoustic waves.[1-4*] Nonlinear interaction between the injected high frequency wave and the signal wave produces modulation sidebands with desirable directivity.

As shown in Fig. 1 the PARRAY consists of two widely spaced transducers: one, called the "pump," which generates a high frequency carrier, and the other, designated the hydrophone, which receives the resultant modulated signal. A receiver demodulates the signal from the hydrophone and produces an electrical output at the signal frequency.

For a collimated planar pump wave, with frequency much higher than the signal, the pressure observed at the hydrophone can be

---

*References are listed in the bibliography.

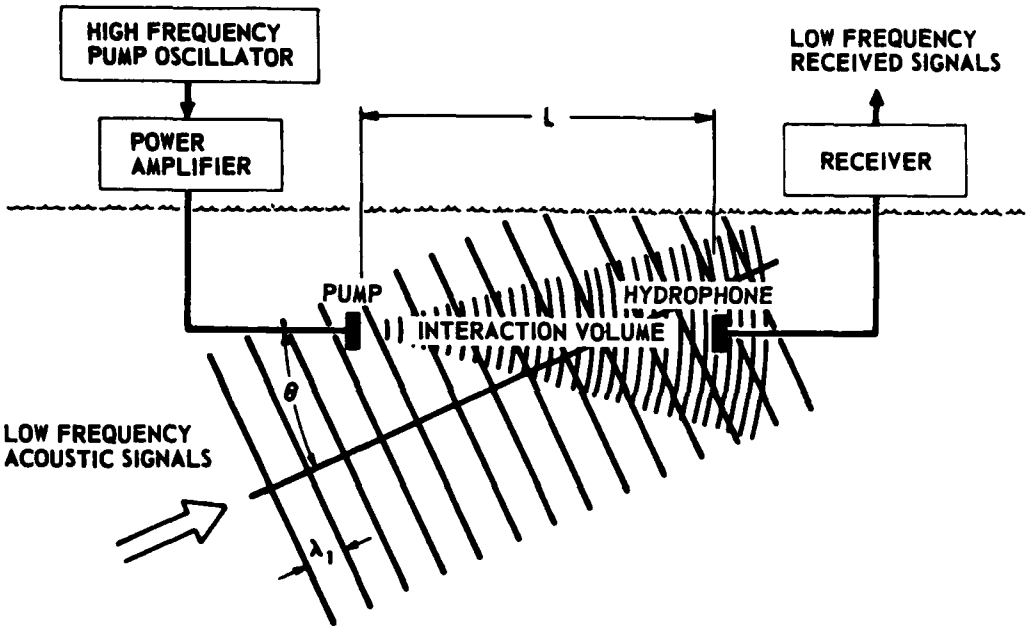

FIGURE 1
PARRAY FUNCTIONAL DIAGRAM

expressed as a phase modulated signal.[5] For a sinusoidal pump wave, $c \cos\omega_o t$, the hydrophone signal is expressed by Reeves et al.[6] as

$$s(t) = c' \cos[\omega_o t + \phi(t) + \psi] \tag{1}$$

where the phase modulating signal $\phi(t)$ is given by:

$$\phi(t) = \frac{\omega_o L\left(\frac{B}{2A} + \cos\theta\right) \sin\left[\frac{\omega_2 L}{2c_o}\left(1-\cos\theta\right)\right]}{\rho_o c_o^3\left[\frac{\omega_2 L}{2c_o}\left(1-\cos\theta\right)\right]} p(t) \quad , \tag{2}$$

where

$p(t)$ = signal pressure at frequency ω_2,

B/A = parameter of nonlinearity of water (≈ 5),

L = distance from pump to hydrophone,

θ = angle of arrival of signal wave with respect to the pump wave,

ρ_o = density of water,

c_o = sound speed;

the pressure at the pump frequency is given by:

$$\rho_o(t,x) = c'(x) \cos\left(\omega_o t - \frac{x}{c_o}\right) \tag{3}$$

and

ψ = the phase constant determined by the pump hydrophone separation.

This equation predicts phase modulation sidebands with directivity much like an end-fired array of length L.[6] Truchard[7] derives a similar result for a spherically spreading pump wave. The acoustic phase modulation

index produced by realistic signal wave amplitudes is extremely small, requiring very sensitive signal processing equipment.

2. Effects of PARRAY Transducer Vibration

Relative motion of the PARRAY transducers along the PARRAY axis causes additional phase modulation of the signals observed at the hydrophone. The motion of the transducers produces an additional term, ϕ_m, in Eq. (1), so that[6]

$$s(t) = c' \cos[\omega_o t+\phi(t)+\phi_m(t)+\psi] \quad , \tag{4}$$

where

$$\phi_m(t) = \frac{2\pi}{\lambda}\left[d_p\left(t - \frac{L}{c_o}\right) - d_h(t)\right] \quad , \tag{5}$$

is the phase modulating signal produced by motion of the transducers, λ is the wavelength of the pump carrier, $d_h(t)$ is the displacement of the hydrophone, and $d_p(t-L/c_o)$ is the displacement of the pump in retarded time. Because $2\pi/\lambda$ is large, the vibration modulation index $(2\pi d/\lambda)$ can be large for relatively small transducer displacement (d). For example, if the pump frequency is 65 kHz, the modulation index is unity for a peak transducer displacement of 3.7 mm.

Due to the nonlinear nature of the phase modulation process intermodulation products are formed by the interaction of the mechanically generated vibration signals and the acoustically generated sidebands. If the vibration modulation index is large, transducer vibration may significantly degrade PARRAY performance.

Transducer vibration produces intermodulation sidebands around each line in the received spectrum. This effect is illustrated in Fig. 2.

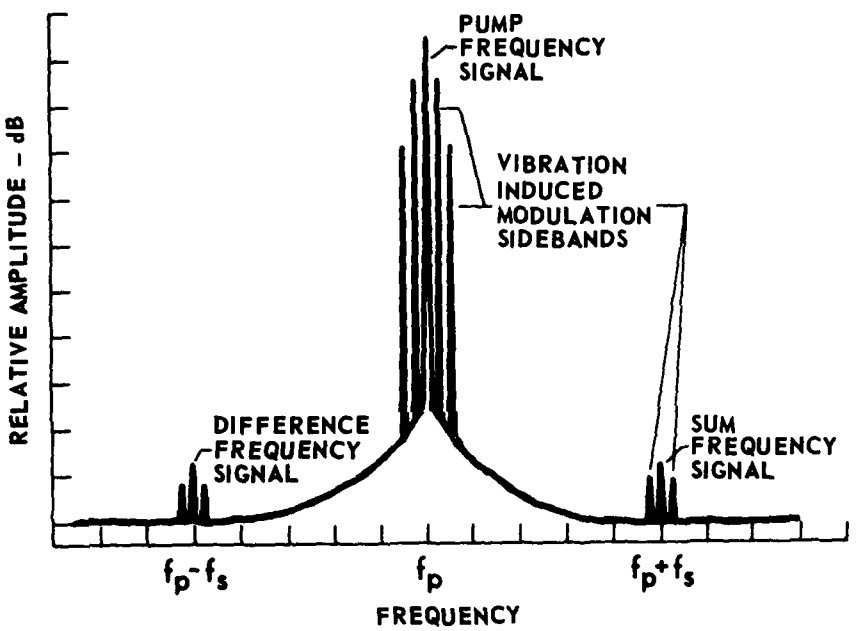

FIGURE 2
PARAMETRIC RECEIVER SPECTRUM
WITH VIBRATING TRANSDUCERS

This intermodulation process can reduce the amplitude of the acoustically generated sidebands and make narrowband acoustic signals difficult to identify. The spectrum produced by phase modulation of a carrier by two sinusoidal signals is derived in Appendix A. As discussed below, a narrowband phase-locked loop (PLL) demodulator can track low frequency phase variations in the received carrier, thus reducing the level of these intermodulation sidebands. Hence, the PLL could strongly enhance the detection of narrowband signals in the presence of high level transducer vibration.

B. Linear PLL Demodulator Theory

A block diagram of a typical PLL demodulator is shown in Fig. 3. The demodulator operates as a closed loop servo system with phase as the controlled variable. The accuracy with which the voltage controlled oscillator (VCO) tracks the input phase variations is a function of the loop gain. Because of the integrating action of the VCO, and the low pass filter in the loop, the loop gain decreases as frequency increases. Changing the loop bandwidth allows the phase locked loop to be adapted to many signal processing applications.

There are two basic types of phase-locked loop demodulators. The first type is the wide band or modulation tracking PLL. The loop bandwidth of this type of PLL encompasses all the modulation frequencies of interest. In this way the VCO phase is allowed to track the phase (or frequency) of the input signal. Normally the output of this type of demodulator is the VCO input port. This type of demodulator is used to demodulate FM signals.

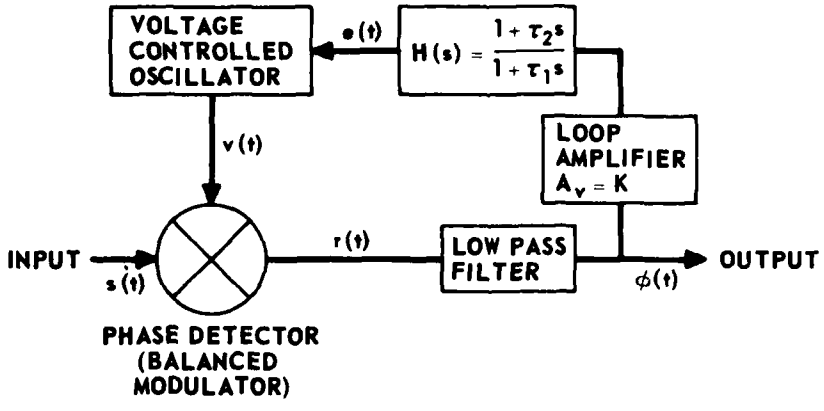

FIGURE 3
PHASE LOCKED LOOP DEMODULATOR

ARL:UT
AS-80-852
RAL-GA
2-28-80

The second type of PLL demodulator is the narrowband or carrier tracking PLL. The loop bandwidth is normally less than the lowest modulation frequency of interest. Because the VCO cannot track the input modulation, the phase error output of the phase detector contains the signals of interest. The carrier tracking PLL is used to demodulate wideband phase modulation signals such as are found in the PARRAY system. In addition, this type of PLL attenuates high level low frequency interference signals and their intermodulation products.

An important parameter for any closed loop control system is system loop gain. Loop gain is closely related to frequency response and stability. Asymptotic (Bode) plots of the magnitude and phase of the loop gain allow quick estimation of loop response and stability. Most phase-locked loop circuits contain a single pole loop low pass filter with phase lead correction to assure stability. However, higher order PLLs (with more than one low pass filter pole) such as described in Refs. 8 and 9 are useful in some applications.

Small signal frequency response of a PLL is readily determined by linearization of the system's equations and Laplace transformation of the resulting differential equation.[10-11] The resulting response equation for the carrier tracking PLL is given by:

$$\phi(s) = \frac{s}{s + K\,F(s)}\,\phi_i(s) = G(s)\,\phi_i(s) \quad , \tag{6}$$

where

$\phi(s)$ = Laplace transform of the phase detector output,

$\phi_i(s)$ = Laplace transform of the input signal phase,

s = Laplace transform variable,

K = dc loop gain,

F(s) = the transfer function of the loop filter.

Equation (6) indicates a high pass characteristic. Because the VCO tracks signal phase, low frequency modulation is attenuated, while higher frequency modulation is not. This linear analysis is exact if all loop components are linear.

C. Intermodulation in PLL Demodulators

Linear analysis predicts no distortion when a PLL demodulates a purely phase modulated carrier. For PARRAY applications with high level transducer vibration, nonlinearities in loop components make this analysis inadequate.

Nonlinearities in PLL circuits produce harmonics of the input signals as well as intermodulation products. Intermodulation performance is especially important for a mobile PARRAY application where the PARRAY demodulator must process low level acoustic signal sidebands in the presence of high level vibration induced sidebands. Deviation from perfect linearity of the phase-locked demodulator will produce intermodulation products which may reduce the PARRAY effectiveness. In the following sections previous work on PLL distortion will be reviewed, and nonlinear differential equations will be solved for the magnitude of intermodulation terms caused by nonlinear phase detector and VCO characteristics in a narrowband PLL.

1. PLL Intermodulation Literature

Although PLL nonlinear operation has been the subject of a number of papers, the majority are concerned with PLL locking phenomena or the effects of noise on the PLL; a recent bibliography of PLL

applications[12] shows that few papers have considered distortion in the PLL demodulator.

Schilling and Smirlock[13] investigated distortion in a modulation tracking PLL demodulator. They used an iterative procedure to derive expressions for PLL distortion caused by nonlinear phase detector characteristics and nonlinearities in VCO tuning response. The effects of the loop filter were neglected in the derivation making the results invalid for a narrowband PLL.

Using unstated assumptions and an iterative technique, Thomas[14] derived an expression for signal distortion due to phase detector or VCO nonlinearities as well as bandpass filter phase nonlinearities. However, the derivation is not applicable to the PARRAY PLL receiver because assumptions were made which are valid only for the modulation tracking PLL.

No derivation has been found in the literature for low frequency intermodulation caused by PLL components in a narrowband loop. Because of the nature of the PARRAY PLL application a separate derivation of the effects of VCO and phase detector nonlinearities will be made.

2. Intermodulation due to Phase Detector Nonlinearities

A block diagram of the phase-locked loop model analyzed was given in Fig. 3. Nonlinearities in the PARRAY PLL occur in the analog multiplier, which acts as a sinusoidal (nonlinear) phase detector, and the nonlinear electronic tuning response of the VCO.

The method used in deriving the effects of PLL nonlinearities is to apply a perturbation series technique. In the derivation it is assumed that the PLL input signal is phase modulated by the sum of a

high level low frequency sinusoid and a lower level high frequency sinusoid that is the desired signal. This receiver input corresponds to the PARRAY hydrophone output which is a carrier signal phase modulated by low level acoustic signals and high level low frequency transducer vibration. The magnitude of intermodulation sidebands produced by the PLL demodulator with a sinusoidal phase detector will be derived below.

The problem of nonlinear phase detectors is of interest because the commonly used type of phase detector produces a sinusoidal characteristic. The double balanced diode mixer has extremely wide dynamic range as well as a very wide bandwidth; however, its phase detector characteristic is sinusoidal. This type of phase detector acts as a multiplier; its output is proportional to the product of the input signals whose relative phase is being compared.

In Fig. 3 s(t) is the phase modulated sinusoidal input signal and v(t) is the VCO output sinusoid. For stable operation with noninverting loop gain, the VCO phase should lead the input phase by approximately 90°. This means that the two sinusoids can be represented as

$$s(t) = \sqrt{2}\,\sin\left(\omega_o t+\phi_i(t)\right) \tag{7}$$

and

$$v(t) = \sqrt{2}\,\cos\left(\omega_o t+\theta_o(t)\right) \quad , \tag{8}$$

where

$\phi_i(t)$ = the input phase modulation signal,

$\theta_o(t)$ = the VCO phase, and

the factor $\sqrt{2}$ has been introduced for convenience in later equations. Using these relations we get the following result for the phase detector output (with implicit time dependence):

$$r(t) = \sin(\phi_i - \theta_o) + \sin(2\omega_o t + \phi_i + \theta_o) \quad . \tag{9}$$

This shows that r(t) is the sum of a high frequency component which is eliminated by the low pass filter and a modulation frequency component. The modulation frequency component of r(t), $\phi(t)$ is given by:

$$\phi(t) = \sin(\phi_i - \theta_o) \quad . \tag{10}$$

Assuming that all loop components except the phase detector are linear, the magnitude of the first order distortion products produced by phase detector nonlinearity can be derived as follows.

Working in the time domain, the nonlinear loop equation can be derived for a loop filter with the following frequency domain transfer of function:

$$F(s) = \frac{1 + \tau_2 s}{1 + \tau_1 s} \quad . \tag{11}$$

The result is the following inhomogeneous second order nonlinear differential equation:[11]

$$\tau_1 \frac{d^2\phi}{dt^2} + [1 + K\tau_2 \cos\phi] \frac{d\phi}{dt} + K \sin\phi = \tau_1 \frac{d^2\phi_i}{dt^2} + \frac{d\phi_i}{dt} \quad . \tag{12}$$

Instead of completely linearizing the equation, the sine and cosine functions are replaced by the first two terms in their power series expansions. Although this approximation requires that the phase error be

less than unity, it is more exact than complete linearization of the loop equations. The resulting simplified nonlinear equation is:

$$\tau_1 \frac{d^2\phi}{dt^2} + \left[1 + K\tau_2\left(1 - \frac{\phi^2}{2}\right)\right]\frac{d\phi}{dt} + K\left(\phi - \frac{\phi^3}{6}\right) = \tau_1 \frac{d^2\phi_i}{dt^2} + \frac{d\phi_i}{dt} \quad . \tag{13}$$

Equation (13) can be solved by assuming a solution for $\phi(t)$ in terms of a power series in the parameter ε, which is small compared to unity:

$$\phi(t) = \sum_{n=0}^{\infty} \varepsilon^n \phi_n(t) \quad . \tag{14}$$

This series solution can be substituted into Eq. (13) and each term in the series evaluated successively.

To proceed, it is convenient to define the form of the input signal phase ϕ_i, and the value of ε. Therefore, assume that the phase of s(t) is given by:

$$\begin{aligned} \phi_1 &= \Delta\omega_o t + A_1 \sin\omega_1 t + A_2 \sin\omega_2 t \\ &= \Delta\omega_o t + 2\pi\varepsilon \sin\omega_1 t + 2\pi\varepsilon \frac{A_2}{A_1} \sin\omega_2 t \quad , \end{aligned} \tag{15}$$

where

$\Delta\omega_o$ = initial frequency offset between the VCO and input signal,

$\varepsilon = A_1/2\pi << 1$,

$\omega_1 << \omega_2$, and

$A_1 >> A_2$.

Equations (14) and (15) allow both sides of Eq. (13) to be put in the form of a general power series in ε. Since the solution, Eq. (14), must be valid for arbitrary ε, the coefficients for each power of ε on both sides of the resulting equation can be equated. The resulting equation for the zero order (in ε) term in the solution is:

$$K\phi_o - \frac{K}{6}\phi_o^3 = \Delta\omega_o \quad . \tag{16}$$

Equation (16) gives the value of the dc output of the phase detector, ϕ_o. For the narrowband loop $\Delta\omega_o/K$ is much less than unity; thus the value of ϕ_o is much less than unity and can be approximated as:

$$\phi_o \approx \frac{\Delta\omega_o}{K} << 1 \quad . \tag{17}$$

Collecting terms of the first order in ε and noting the inequality in Eq. (17), the following equation for ϕ_1 (in the frequency domain) can be derived:

$$\varepsilon\phi_1(s) = \frac{s(1+\tau_1 s)}{(1+\tau_1 s) + K(1+\tau_2 s)}\,\phi_i(s) = \frac{s}{s + KF(s)}\,\phi_i(s)$$

$$= G(s)\phi_i(s) \quad . \tag{18}$$

Thus the second term in the series solution for the PLL output given in Eq. (18) is identical to the linear PLL output, Eq. (6). By replacing s with $j\omega$ in Eq. (18) and combining it with the assumed form of the input, Eq. (15), the first order time function is obtained:

$$\varepsilon_1(t) = \mathrm{Re}\left\{-jA_1G(j\omega_1)\, e^{j\omega_1 t} - jA_2G(j\omega_2)\, e^{j\omega_2 t}\right\} \quad , \tag{19}$$

where $\mathrm{Re}\{\ \}$ denotes the real part of a complex quantity.

The second order equation in ε can be solved for the magnitude of the first order distortion products. These distortion products include second harmonics of the input signal and first order intermodulation products (sum and difference frequencies). However, the intermodulation products are of interest here, and only their magnitudes will be retained.

Assuming an input of the form given in Eq. (15), the intermodulation terms are given by:

$$\varepsilon^2\phi_2|_{IM} = \mathrm{Re}\left\{-jC_1\, e^{j\omega_s t} - jC_2\, e^{j\omega_d t} + C_3\, e^{j\omega_s t} + C_4\, e^{j\omega_d t}\right\} \quad . \tag{20}$$

$$\omega_s = \omega_2 + \omega_1 \quad , \tag{21}$$

$$\omega_d = \omega_2 - \omega_1 \quad . \tag{22}$$

In this result, $|_{IM}$ denotes the intermodulation terms, and

$$C_1 = \frac{\frac{1}{4}\,\Delta\omega_o\, A_1A_2G(j\omega_1)\, G(j\omega_2)\tau_2\omega_2 + (1+K\tau_2)\omega_s C_3}{\left(K-\tau_1\omega_s^2\right)} \quad , \tag{23}$$

$$C_2 = \frac{\frac{1}{4}\,\Delta\omega_o\, A_1A_2G^*(j\omega_1)\, G(j\omega_2)\tau_2\omega_2 + (1+K\tau_2)\omega_d C_4}{\left(K-\tau_1\omega_d^2\right)} \quad , \tag{24}$$

$$C_3 = \frac{\Delta\omega_o\left[\frac{1}{2}(1+K\tau)\tau_2\omega_2\omega_s + \left(K-\tau_1\omega_s^2\right)\right]}{2\left[\omega_s^2(1+K\tau_2)^2 - \left(K-\tau_1\omega_s^2\right)^2\right]} A_1G(j\omega_1)A_2G(j\omega_2) \tag{25}$$

$$C_4 = \frac{-\Delta\omega_o\left[\frac{1}{2}(1+K\tau_2)\tau_2\omega_2\omega_d + \left(K-\tau_1\omega_d^2\right)\right]}{2\left[\omega_d^2(1+K\tau_s)^2 + \left(K-\tau_1\omega_d^2\right)^2\right]} A_1G^*(j\omega_1)A_2G(j\omega_2) \quad , \tag{26}$$

where * denotes the complex conjugate of a complex quantity.

Because the terms of Eq. (20) are in phase quadrature, the total magnitude of the intermodulation products at frequency ω_s is given by:

$$|IM| = \sqrt{C_3^2 + C_1^2} \quad . \tag{27}$$

If ω_d is approximately equal to ω_s, the intermodulation products at each frequency have approximately the same magnitudes.

Equations (20)-(27) give the magnitude and phase of the first order intermodulation sidebands present at the output of the sinusoidal phase detector for a PLL with input phase given by Eq. (15). This type of result, where the first order sidebands are proportional to the initial frequency offset, is predicted by Blanchard.[15]

Examination of this result will prove useful. First, note that $|A_1G(j\omega_1)|$ and $|A_2G(j\omega_2)|$ in Eqs. (21)-(24) are the magnitudes of the outputs of the phase detector at frequencies ω_1 and ω_2, respectively. Thus, the magnitude of the first IM sidebands is proportional to the product of the magnitudes of the linear outputs at the frequencies combining to form the IM distortion products. Also note that since $|A_2G(j\omega_2)|$ is the magnitude of the signal at frequency ω_2, Eq. (27) can

be normalized with respect to $|A_2G(j\omega_2)|$ to give a comparison between the IM distortion levels at the PLL output and the signal of interest.

Because a narrowband loop is assumed and the value of $\Delta\omega_o$ is on the order of unity, the magnitude of this normalized distortion is much less than $|(A_1G(j\omega_1)|$. For the PLL examined experimentally in this investigation, distortion due to VCO nonlinearity was significantly larger than the distortion caused by phase detector nonlinearity derived above. For this reason the effect of VCO nonlinearity will be derived next.

3. Intermodulation Due to Nonlinear Voltage Controlled Oscillator

Intermodulation distortion is also caused by nonlinearity of the VCO voltage-to-frequency characteristic. This nonlinearity causes the linearizing assumptions used in the linear PLL derivation to be less accurate. To determine the levels of intermodulation produced by VCO nonlinearity a perturbation solution of the nonlinear PLL equations is derived. In this derivation it is assumed that the VCO output can be modeled as a phase modulated wave of the form

$$s(t) = \sqrt{2}\cos[\omega_o t+\theta_o(t)] \quad , \tag{28}$$

where $\theta_o(t)$ can be approximated by:

$$\phi_o(t) = \int_o^t e(t)dt + A\int_o^t [e(t)]^2dt + B\int_o^t [e(t)]^3dt \quad , \tag{29}$$

where e(t) is the tuning voltage at the VCO input. Also it is assumed that the loop filter transfer function can be approximated by:

$$F(s) = \frac{1+\tau_2 s}{\tau_1 s} \quad . \tag{30}$$

This means that $\omega\tau_1$ must be much greater than unity, an assumption that will be violated for some loop filter and input frequency combinations.

Assuming the phase error $(\phi_i-\theta_o)$ is small compared to unity, the phase detector output given in Eq. (10) can be linearized by approximating the sine by its argument. Combining this result with Eqs. (28)-(30) and with Eq. (7), an approximate equation governing the system can be obtained. This equation (with implicit time dependence) is:

$$\phi + \frac{K}{\tau_1}\int_o\left[\int_o^t \phi dt + \tau_2\phi\right]dt + \frac{AK^2}{\tau_1^2}\int_o^t\left[\int_o^t \phi dt + \tau_2\phi\right]^2 dt$$

$$+ \frac{BK^3}{\tau_1^3}\int_o^t\left[\int_o^t \phi dt + \tau_2\phi\right]^3 dt = \phi_i \quad . \tag{31}$$

Differentiating with respect to time simplifies the form of Eq. (31). By assuming a solution in the form of a power series as before, a series of recursive formulas can be obtained and solved for each term in the series solution given by Eq. (14). Several important assumptions must be made in order to simplify the equations for each term in Eq. (14). These assumptions are

(1) only the steady state solution is sought,

(2) static phase error is relatively constant--oscillators operate at nearly the same frequency and K is large (by assuming a perfect integrator in the PLL, the static phase error will be zero), and

(3) the following inequalities are valid:

$$\frac{2AK}{\tau_1}\left(\int\phi_o dt\right) \ll 1 \tag{32}$$

$$\frac{3BK^3}{\tau_1^2}\left(\int \phi_o dt\right)^2 << 1 \quad , \tag{33}$$

$$\frac{1}{\omega_1} << \tau_2 \quad . \tag{34}$$

These assumptions allow the first two terms of the series solution, Eq. (14), to be determined. These terms are identical to the solution predicted by linear PLL analysis. The first term in the series solution (dc term) is zero, since there is a perfect integrator in the PLL. However, the integral of this dc term is given by:

$$\lim_{t \to \infty} \int_o^t \phi_o dt = \frac{\tau_1 \Delta\omega_o}{K} \quad . \tag{35}$$

The second term in the series solution for ϕ is given by:

$$\varepsilon\phi_1(s) = \frac{\tau_1 s^2}{\tau_1 s^2 + K(1+\tau_2 s)} \phi_i(s) = G(s)\phi_i(s) \quad . \tag{36}$$

This term is identical to the solution predicted by the linear PLL equation, Eq. (6), for the PLL filter described by Eq. (30).

Using Eqs. (32)-(34), the magnitude of the intermodulation products contained in the next term of the series solution can be determined. If the input signal ϕ_i is given by Eq. (15), the intermodulation terms will be given by:

$$\varepsilon^2\phi_2\big|_{IM} = \mathrm{Re}\left\{-jC_1 e^{j\omega_s t} - jC_2 e^{j\omega_d t} + C_3 e^{j\omega_s t} + C_4 e^{j\omega_d t}\right\} \quad , \tag{37}$$

where

$$C_1 = \frac{AK^2 G(j\omega_1)\, G(j\omega_2) A_1 A_2 - C_3\, K\tau_2 \tau_1 \omega_1 \omega_2}{\tau_1^2 \omega_1 \omega_2 \left(\omega_s - \frac{K}{\tau_1 \omega_s}\right)} \quad , \tag{38}$$

$$C_2 = \frac{-\left[AK^2 A_1 G^*(j\omega_1)\, A_2 G(j\omega_2) + K\tau_2 \tau_1 \omega_1 \omega_2\, C_4\right]}{\tau_1^2 \omega_1 \omega_2 \left(\omega_d - \frac{K}{\tau_1 \omega_d}\right)} \quad , \tag{39}$$

$$C_3 = \frac{-\, AK^2 \tau_2 \left[\omega_2 \left(\omega_s - \frac{K}{\tau_1 \omega_s}\right) - \frac{K}{\tau_1}\right]}{\tau_1^2 \omega_1 \omega_2 \left[\left(\omega_s - \frac{K}{\omega_s \tau_1}\right)^2 + \left(\frac{K\tau_2}{\tau_1}\right)^2\right]} A_1 G(j\omega_1)\, A_2 G(j\omega_2) \quad , \tag{40}$$

$$C_4 = \frac{AK^2 \tau_2 \left[\omega_2 \left(\omega_d - \frac{K}{\tau_1 \omega_d}\right) + \frac{K}{\tau_1}\right]}{\tau_1^2 \omega_1 \omega_2 \left[\left(\omega_d - \frac{K}{\tau_1 \omega_d}\right)^2 + \left(\frac{K\tau_2}{\tau_1}\right)^2\right]} A_1 G^*(j\omega_1)\, A_2 G(j\omega_2) \quad . \tag{41}$$

Equations (37)-(41) describe the magnitude and phase of the first order intermodulation sidebands produced by a PLL with a nonlinear VCO characteristic given by Eq. (29). The derivation requires that the loop filter have a transfer function that can be approximated by Eq. (30) and that the input be of the form given in Eq. (15).

For the circuit described in the next chapter, it can be shown that the magnitudes of the upper and lower intermodulation sidebands should be almost equal. Therefore, in the next chapter data obtained by measurement of the PLL intermodulation distortion will be compared with results of calculations using Eqs. (37)-(41) for the upper sideband. It should be noted that some of the data were taken

under conditions that violate the assumptions made in the preceding derivation. These data will be compared with theoretical predictions after normalizing with respect to input modulation index, A_1, and output signal level, $A_2G(j\omega_2)$.

D. Effects of Amplitude Modulation on a PLL Demodulator

The response of a PLL demodulator to an amplitude modulated signal is of interest because PARRAY signals are often amplitude as well as phase modulated. This amplitude modulation (AM) can be caused by variations in propagation conditions, variations in transducer alignment, fluctuations in the medium, or VCO amplitude fluctuations.

Because most phase detectors are amplitude sensitive, amplitude modulation of the input produces AM at the PLL output. This result is shown by Gardner[16] for a PLL with no low pass filter. Low frequency amplitude fluctuations in the received signal cause a definite degradation in PARRAY performance in a manner similar to low frequency phase modulation. These effects include formation of modulation sidebands around lines in the received spectrum, and reduction in level of these lines. A carefully designed limiter or AGC circuit at the PLL input should greatly reduce the effects of an amplitude modulated input.

E. Summary of Theoretical Development

In this chapter a number of analytical results have been derived or referenced for a narrowband PLL demodulator. Two of these results will be compared with experimental data in the next chapter. Theoretical results derived or referenced here include linear frequency response, intermodulation caused by nonlinear phase detector characteristics, intermodulation caused by VCO nonlinearities, and PLL response to

amplitude modulation. In the next chapter predictions for linear frequency response and intermodulation due to VCO nonlinearities are compared with experimental data, and results of a test of a PLL demodulator in a PARRAY are described.

CHAPTER III

EXPERIMENTAL INVESTIGATION

The purposes of the experimental investigation were to measure the characteristics of the PLL receiver, compare the attenuation of intermodulation sidebands with theoretical prediction from Chapter II, and evaluate a PLL receiver with PARRAY signals. This chapter includes a description of the types of PARRAY receivers used in the past, description of the PLL circuit tested, and measurement of circuit performance through electronic and acoustic tests.

A. PARRAY Receivers

Before describing performance of the PLL receiver, the signal processing problem and the types of receivers that have been used with the PARRAY will be described. Because of the inefficiency of the acoustic modulation process in water (typically 1%), PARRAY signals are composed of a very high level carrier plus low level modulation sidebands; for example, sideband-to-carrier ratios greater than -165 dB have been measured.[17] The relative magnitude of these signals and their close proximity in frequency makes the PARRAY signal processing problem a formidable one.

Three basic types of receivers have been considered or used for detecting PARRAY sideband information. These receiver types are the bandpass receiver, the carrier rejection (notch filter) receiver, and the phase locked loop receiver.[17-19]

The bandpass receiver is probably the simplest type of receiver to construct. This type of receiver uses one or more bandpass filters to pass the sideband frequencies of interest and greatly attenuate the unwanted carrier. Problems with design occur when low frequency sideband information is desired. To extract low frequency sideband information high Q bandpass filters must be used, thus limiting the frequency range that can be examined.

Because of limitations of the bandpass receiving technique, notch filter receivers have been frequently used to process PARRAY sideband signals.[17] This type of receiver uses high Q crystal filters to sharply attenuate a narrow frequency range at the PARRAY carrier frequency. Typical crystal filters used in this manner will attenuate the PARRAY carrier by more than 60 dB with a notch 8 to 80 Hz wide centered about a 65 kHz center frequency. This type of receiver has been used to measure noise greater than 170 dB below the carrier level at frequencies as close as 50 Hz from the carrier frequency. The disadvantages of this type receiver are its sensitivity to the effects of transducer vibration and its use of specialized crystal filters, which reduce the ability to change carrier frequency and low frequency response.

A third type of receiver that has been proposed[19] for demodulating the PARRAY signals is a phase-locked loop receiver. This receiver uses a phase locked oscillator to directly demodulate phase modulated or frequency modulated signals. This type of circuit is often used to measure phase noise in precision oscillators.[20-24] This technique is useful for the PARRAY application because it can reduce the effects of transducer

vibration, is capable of low noise operation, and allows the frequency response and carrier frequency to be easily changed.

A block diagram of the PLL receiver is shown in Fig. 4. This diagram is similar to the general PLL demodulator shown in Fig. 3 except for the addition of an input matching transformer and the use of low noise components. Calibration oscillators, variable gain output stages, and selectable loop filter components have been added. A detailed description of circuit components and a schematic diagram are included in Appendix B. In the following sections, electronic and acoustic tests of this receiver will be described along with results of these tests.

B. Electrical Measurements of the PLL Receiver

A number of electronic measurements were performed to determine the characteristics of the PLL receiver. Measurements were made of frequency response, receiver noise, and intermodulation distortion. The following sections contain descriptions of the methods used in these measurements as well as comparisons of data and theory where possible.

1. Frequency Response

Receiver frequency response was measured to verify operation of the PLL according to linear theory, and to calibrate the receiver's response. Frequency response was measured by connecting a phase modulated signal of known modulation index to the PLL receiver input, and measuring the amplitude of the modulation frequency at the PLL output. To determine the frequency response, measurements were made at the output of the low noise amplifier to avoid low frequency rolloff caused by later capacitively coupled stages. The resulting frequency response curves are shown in Fig. 5 for low pass filter cutoff frequencies of 0.1 Hz and 10 Hz. The

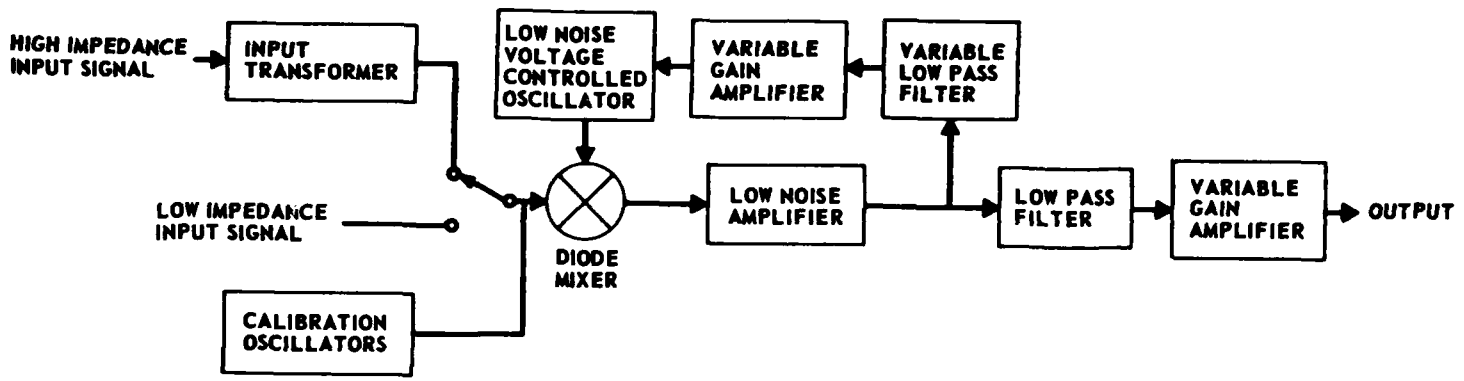

FIGURE 4
EXPERIMENTAL PLL RECEIVER BLOCK DIAGRAM

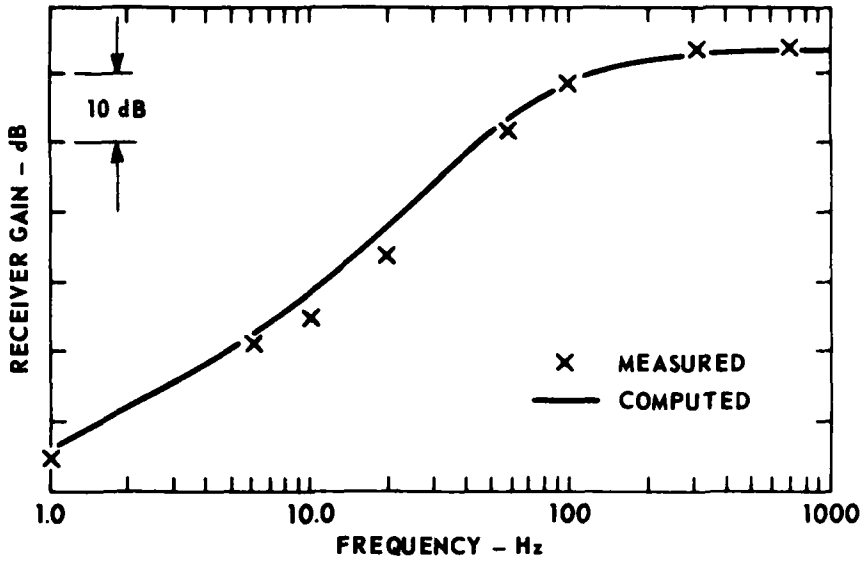

(a) PLL RECEIVER RESPONSE - 10 Hz FILTER

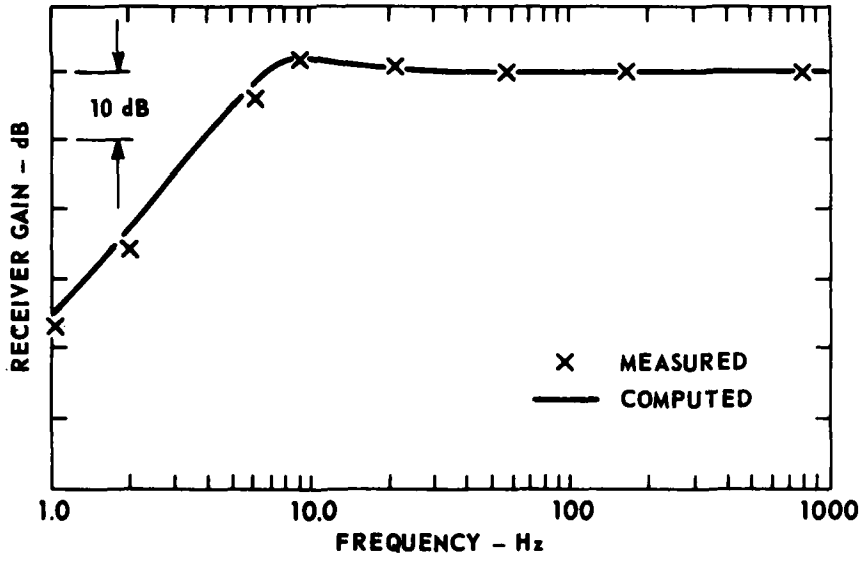

(b) PLL RECEIVER - 0.1 Hz FILTER

FIGURE 5
FREQUENCY RESPONSE OF PLL RECEIVER

measurements agree well with predictions of the linear PLL frequency response calculated using Eq. (6). The slight frequency shift between the computed and the measured values was probably caused by inaccuracies in selecting loop filter components.

2. Intermodulation

The purpose of these measurements was to determine the amount of intermodulation present at the PLL receiver output for an input similar to that expected from a PARRAY undergoing transducer vibration. The magnitudes of the intermodulation products generated by PLL receiver nonlinearities were measured by demodulating a 65 kHz sinusoid phase modulated by the sum of two sinusoids. The measurement method used is described below and experimental intermodulation data are compared with theoretical results from the preceding chapter.

Nonlinearity of the VCO was the major cause of intermodulation distortion in the PLL receiver described in this chapter. To apply theoretical results from the preceding chapter, measurements of the VCO voltage-to-frequency characteristic were made (Fig. 6); these were approximated by a cubic polynomial. The cubic and quadratic coefficients of the polynomial were then divided by the magnitude of the linear coefficient to provide the coefficients A and B (see Eq. (29)) used to calculate expected intermodulation sideband levels. To avoid the highly nonlinear region at the upper end of the VCO characteristic shown in Fig. 6, only the input voltage range from -8.5 to +8.5 V was considered in the cubic approximation. This selection of data is reasonable because the PLL receiver was usually tested with input modulation indices such that only this limited region of the VCO characteristic was used. Using

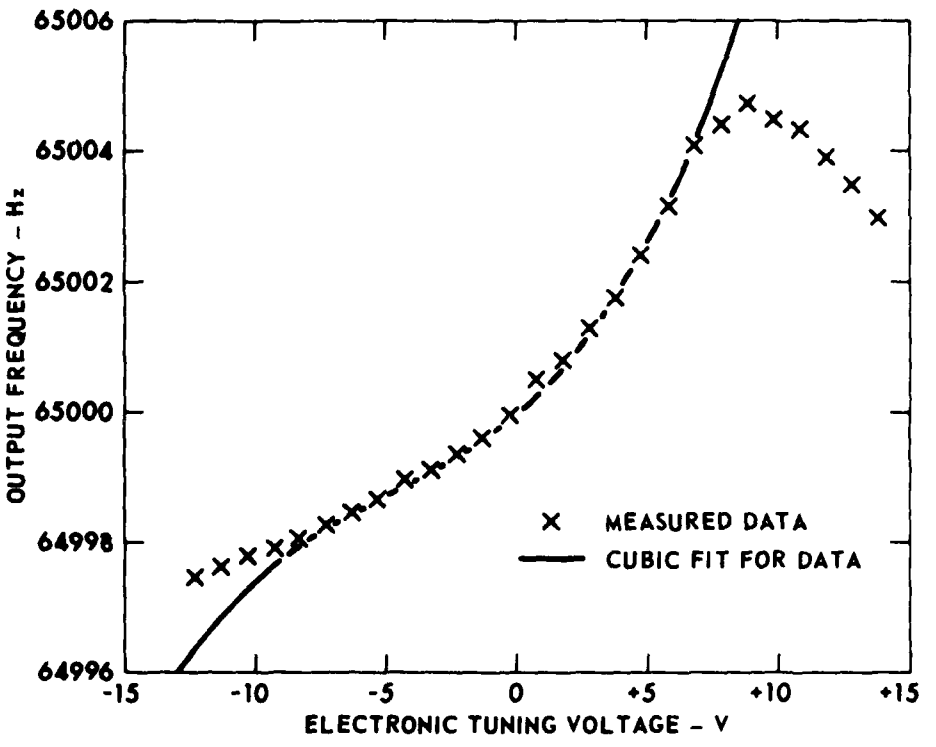

FIGURE 6
VOLTAGE CONTROLLED OSCILLATOR RESPONSE

coefficients of VCO nonlinearity from the curve fitting routine, and Eqs. (37)-(41) from Chapter II, intermodulation levels expected at the PLL output were predicted and compared with the experimental data. Measurements and comparisons with computer calculations are described below.

The measurement system consisted of a Wavetec Model 148 modulated signal generator, and two oscillators used as modulation sources. The external modulation sources were summed using a 600 Ω attenuator for decoupling. Measurement of the frequency spectrum at this summing point confirmed that the summing process and spectrum analyzer were linear.

The spectrum of the phase modulation (PM) generator output was used to determine the levels of the modulation sidebands. Because these levels are not a function of modulation frequency (as predicted by PM theory[25]) the modulation frequency could be raised to allow measurement of the sideband levels on a broadband spectrum analyzer.

Typical modulation indices used for these tests were 0.6 and 0.01 for the low and high frequency tones, respectively. The low modulation frequency ranged from 0.3 to 4 Hz, and the high modulation frequency was 150 Hz. PLL intermodulation performance was measured by comparing the levels of the intermodulation sidebands present at the PLL output with those present at the PLL input. Measured attenuation of intermodulation sidebands is given in Figs. 7-9 for three PLL low pass filter cutoff frequencies. Theoretical predictions for these data are included in Figs. 7 and 8.

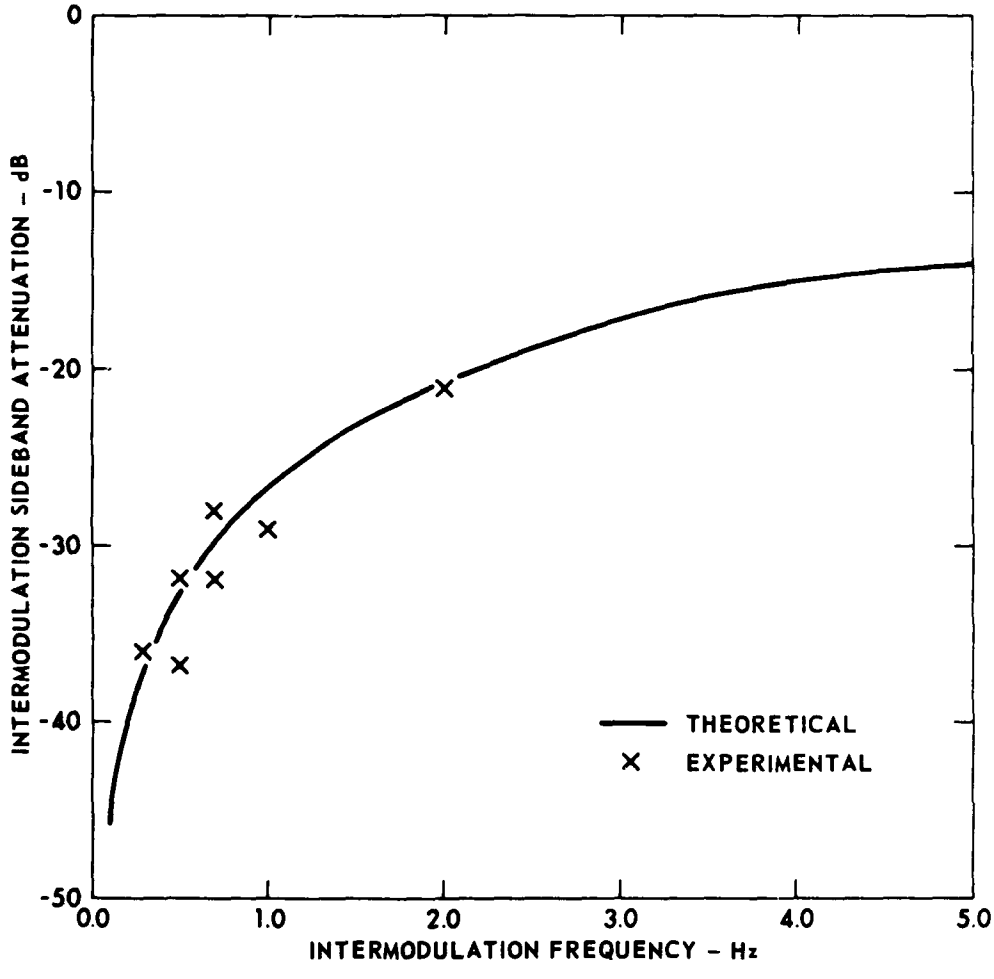

FIGURE 1
PLL INTERMODULATION PERFORMANCE - 0.025 Hz LOOP FILTER

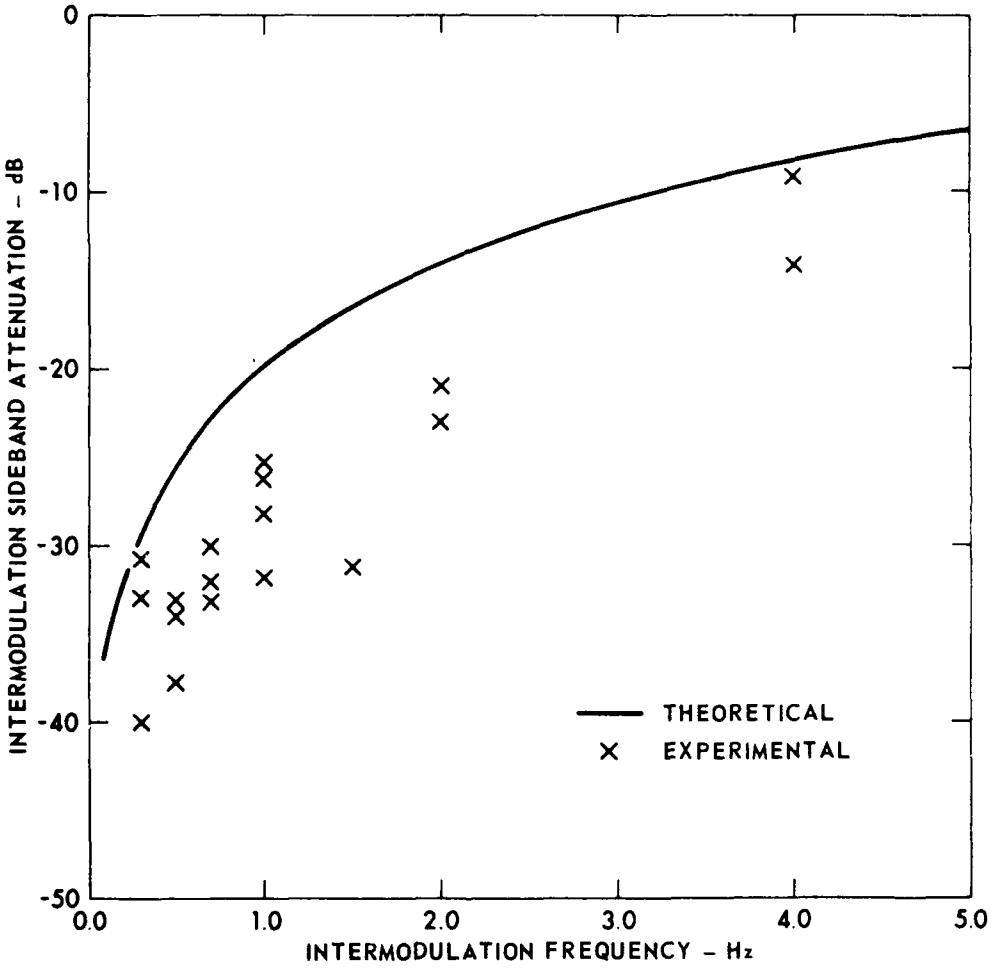

FIGURE 2
PLL INTERMODULATION PERFORMANCE - 0.1 Hz LOOP FILTER

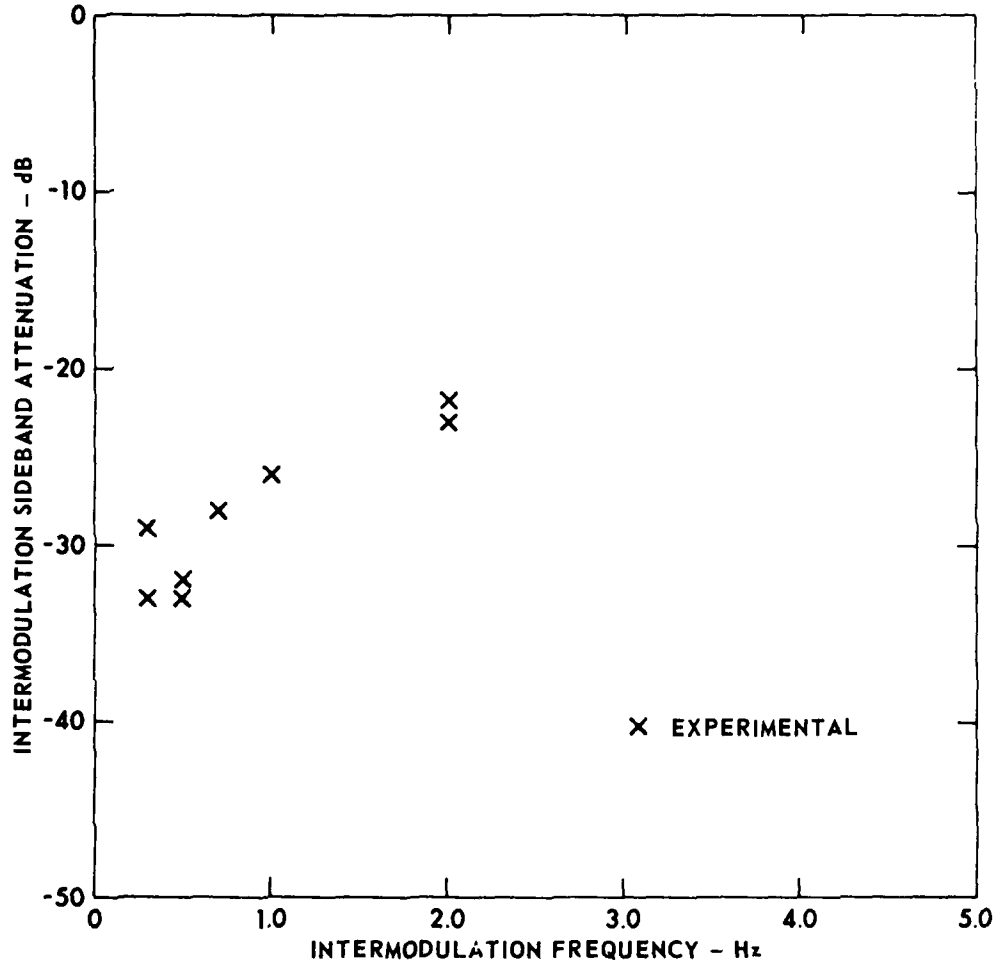

FIGURE 3
PLL INTERMODULATION PERFORMANCE - 10 Hz LOOP FILTER

Figure 7 shows the intermodulation sideband attenuation as a function of frequency, for a low pass filter with cutoff frequency of 0.025 Hz. These data show good agreement with predicted values (solid curve).

Figure 8 shows analogous data for a low pass filter with cutoff frequency of 0.1 Hz. Although none of the assumptions used in the derivation of the theory were violated, it can be seen from Fig. 8 that the PLL receiver attenuated the sidebands more than theory predicts.

Figure 9 shows measured attenuation of intermodulation sidebands for a 10 Hz loop filter. Because the assumptions used in deriving the theory are invalid (particularly Eq. (30)), a theoretical curve based on the analysis presented in Chapter II is not presented. However, these data are shown since the 10 Hz filter was used for acoustic experiments described later.

Figures 7-9 show performance of the PLL receiver in reducing intermodulation produced by demodulation of a signal phase modulated by the sum of a high level, low frequency sinusoid, and a low level, higher frequency signal of interest. Signals of this type are expected at the output of a PARRAY hydrophone with transducer vibration present.

3. Receiver Noise

Electronic noise in the PLL receiver can have a direct effect on PARRAY minimum detectable acoustic levels. Because of the inefficiency of the PARRAY reception process, the sideband signals of interest are far below the carrier level. In these tests the electronic noise of the PLL receiver was measured under realistic operating conditions.

Three major components were expected to limit noise performance: the diode phase detector, the low noise amplifier, and the VCO. The noise of the amplifier and VCO can be measured independently to give a good indication of their contribution to total receiver noise.

Receiver noise was measured by connecting a low noise 65 kHz oscillator to the receiver high impedance input. The mixer input voltage at 65 kHz was measured, and the spectrum of the receiver output plotted. The receiver gain was calibrated earlier; however, additional confirmation of receiver gain was made with the internal calibration oscillators.

The results of the receiver noise tests are shown in Fig. 10. The values plotted are noise level in a 1 Hz band over the frequency range from 30 Hz to 1 kHz referred to the level of the 65 kHz carrier at the receiver input. The noise performance shown here is similar to that reported in Refs. 20 and 22 for a PLL used for oscillator phase noise measurement. However, present band elimination receivers developed for use with the PARRAY are capable of detecting signals in excess of 170 dB below the input carrier amplitude.[17]

4. Summary of Electrical Evaluation

The purpose of the electrical evaluation was to confirm that the PLL receiver operates as predicted. Measurements were made of frequency response, intermodulation performance, and electronic noise. Reasonable agreement was found between theory and experiment for frequency response and intermodulation performance. Noise levels were similar to those of other PLL phase noise measurement systems; however, they were significantly higher than that of presently used notch filter receivers.

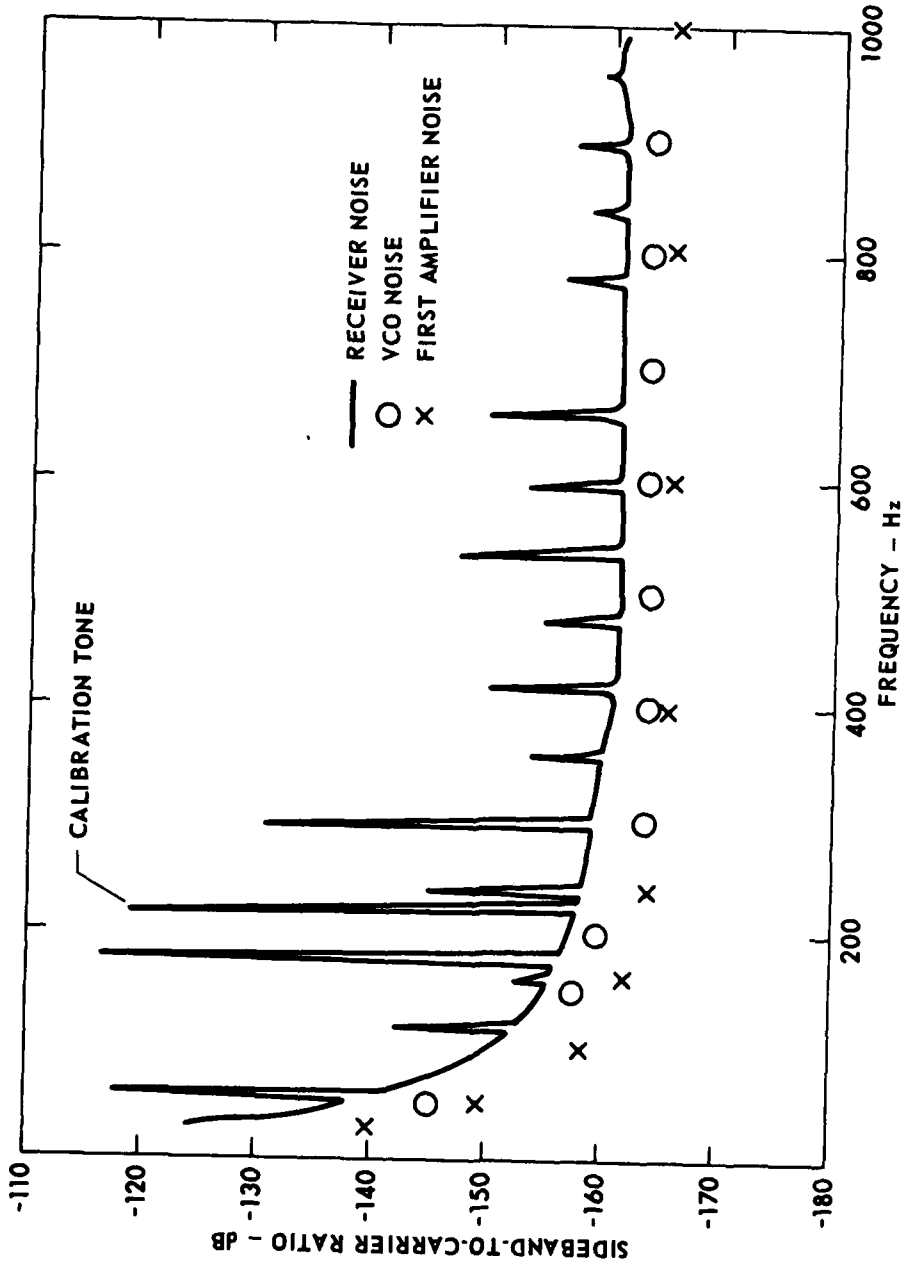

FIGURE 10
PLL RECEIVER NOISE

C. Acoustic Evaluation

Acoustic measurements were performed to evaluate the PLL receiver as part of a PARRAY system with a vibrating hydrophone. These tests were performed using transducers suspended from a floating barge at Applied Research Laboratories' Lake Travis Test Station. The results of these tests demonstrated the effectiveness of a PLL as part of a PARRAY with vibrating transducers.

1. Experimental Apparatus

A general block diagram of the acoustic system is shown in Fig. 11. The system consisted of a low frequency acoustic source and a PARRAY with a vibrating hydrophone. The PARRAY transducers were mounted on columns at a depth of 4.2 m and were separated by 14.9 m. A low frequency sound source (NRL/USRD type J13) was located approximately 2 m behind the pump at the same depth. This sound source projected low frequency sound to be received by the PARRAY. The PARRAY transducers were planar arrays of the type described in Ref. 26. The half-power beamwidth of the arrays was 10° at 65 kHz.

Vibration of the hydrophone was accomplished as shown in Fig. 12. Sinusoidal motion was generated by the motor and eccentric cam, and this motion was transmitted to the underwater components by means of a steel cable. Cable tension was maintained by a 10 kg mass (not shown) mounted to the horizontal part of the L shaped lever. The transducer oscillated back and forth horizontally in a V shaped groove on nylon bushings.

A Systron Donner model 43A-1-A accelerometer was mounted to the hydrophone to measure acceleration along the PARRAY axis. This accelerometer has a frequency range dc to 100 Hz.

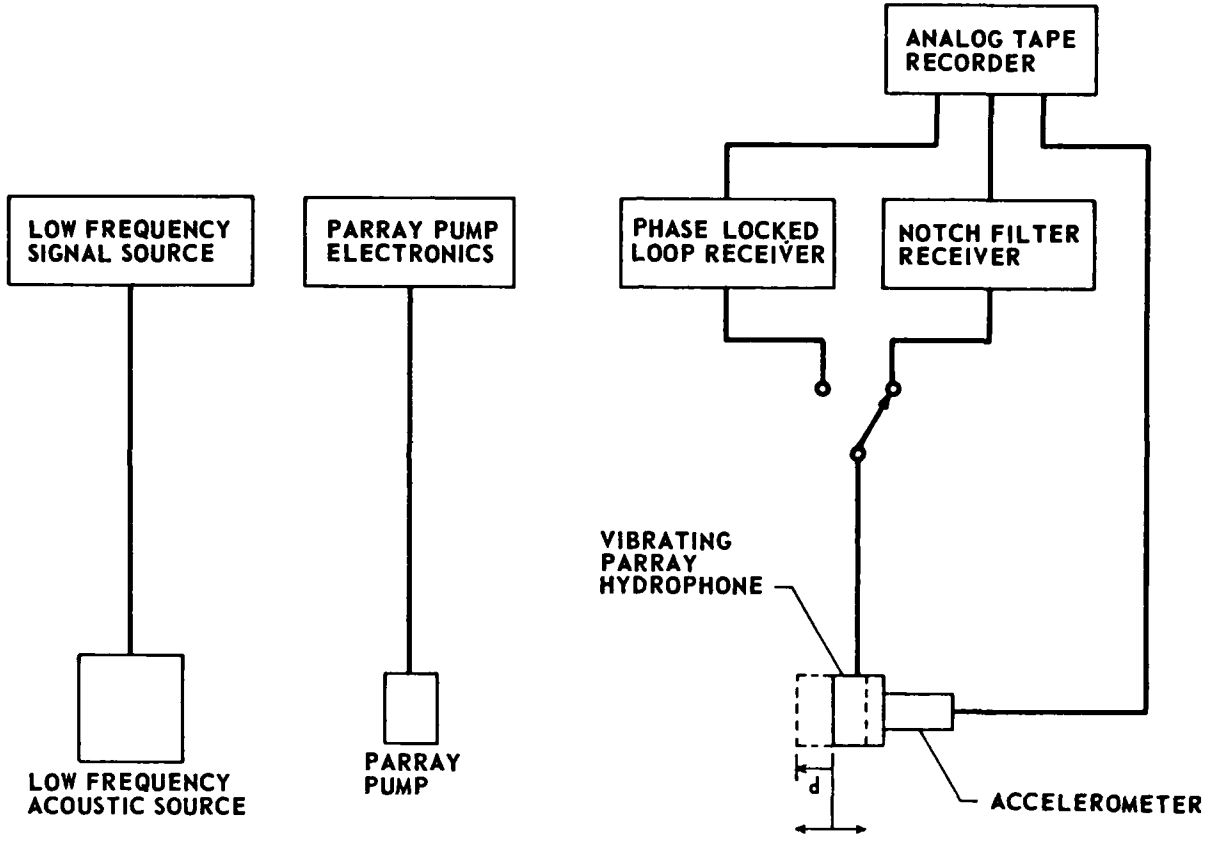

FIGURE 11

BLOCK DIAGRAM OF PARRAY VIBRATION EXPERIMENT

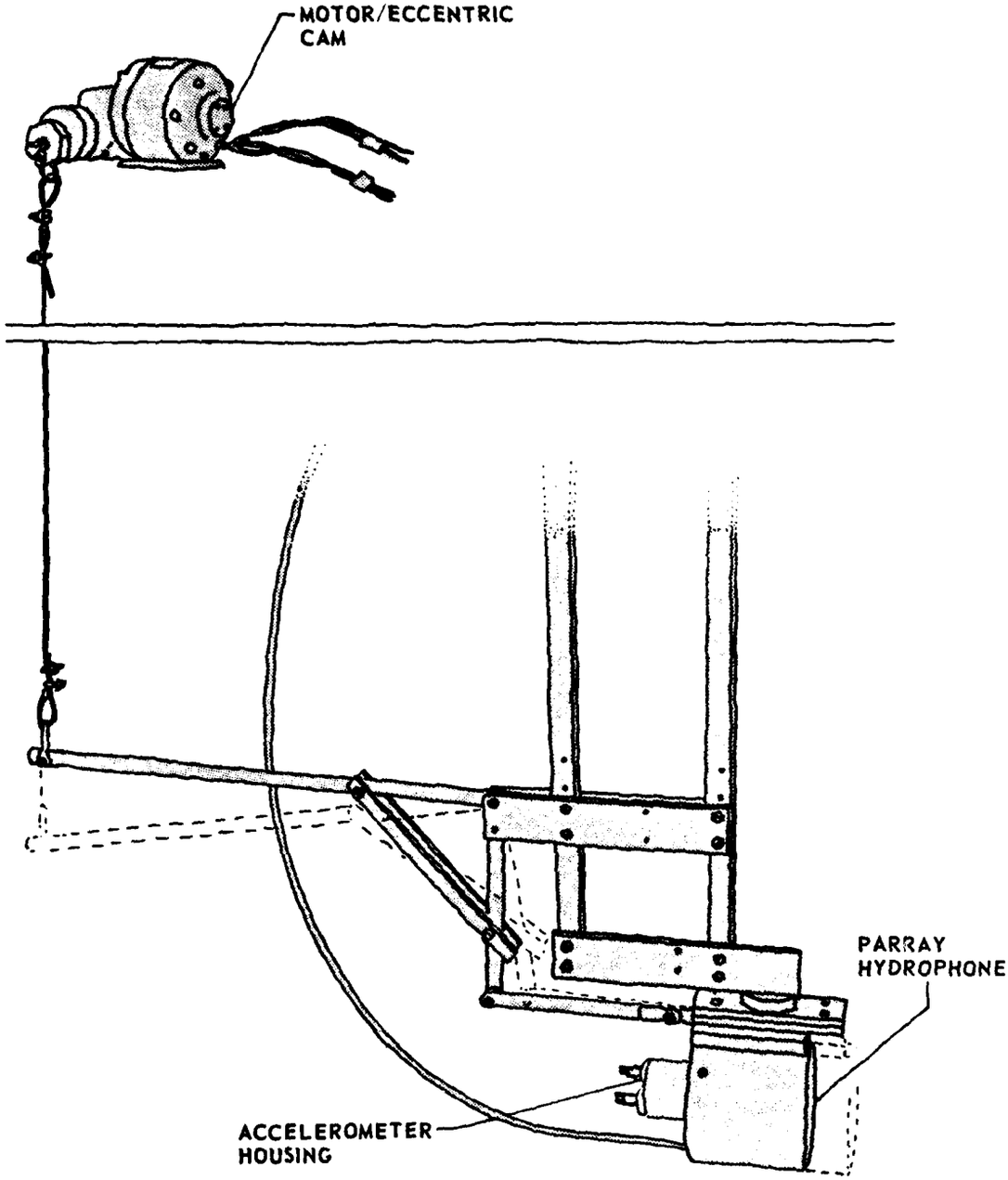

FIGURE 12
TRANSDUCER VIBRATING HARDWARE

The vibration system was capable of producing transducer motion at frequencies from 0.4 to 0.9 Hz, at peak amplitudes from 0.1 to 1 cm in four discrete steps. Backlash at the bearing surfaces reduced the repeatability of the vibration amplitudes. An additional problem was lack of stiffness in the mounting hardware which caused angular misalignments of the narrowbeam hydrophone. These misalignments produced amplitude modulation of the received signals.

Figure 13 is a block diagram of the instrumentation used. With the PARRAY hydrophone vibrating, its output was switched between a notch filter receiver and a PLL receiver with a 10 Hz cutoff loop filter. In this way relative levels of intermodulation for each receiver could be measured under similar conditions.

2. Acoustic Measurements

Acoustic tests were performed by generating a 70 Hz signal in the water and receiving this with the PARRAY. Vibrating the PARRAY hydrophone caused intermodulation between the acoustic phase modulation sidebands and the vibration phase modulation sidebands.

As shown in Fig. 13, a number of different signals were recorded during this test for later analysis. Narrowband spectrum analysis of the recorded data allowed comparisons to be made between the PLL receiver intermodulation signals and the notch filter receiver intermodulation signals. These data were also correlated wtih accelerometer measurements to show the effect of vibration amplitude on intermodulation sideband level.

Spectrum analyses of the outputs of each receiver are shown in Figs. 14 and 15. The curves in these figures show the relative levels of

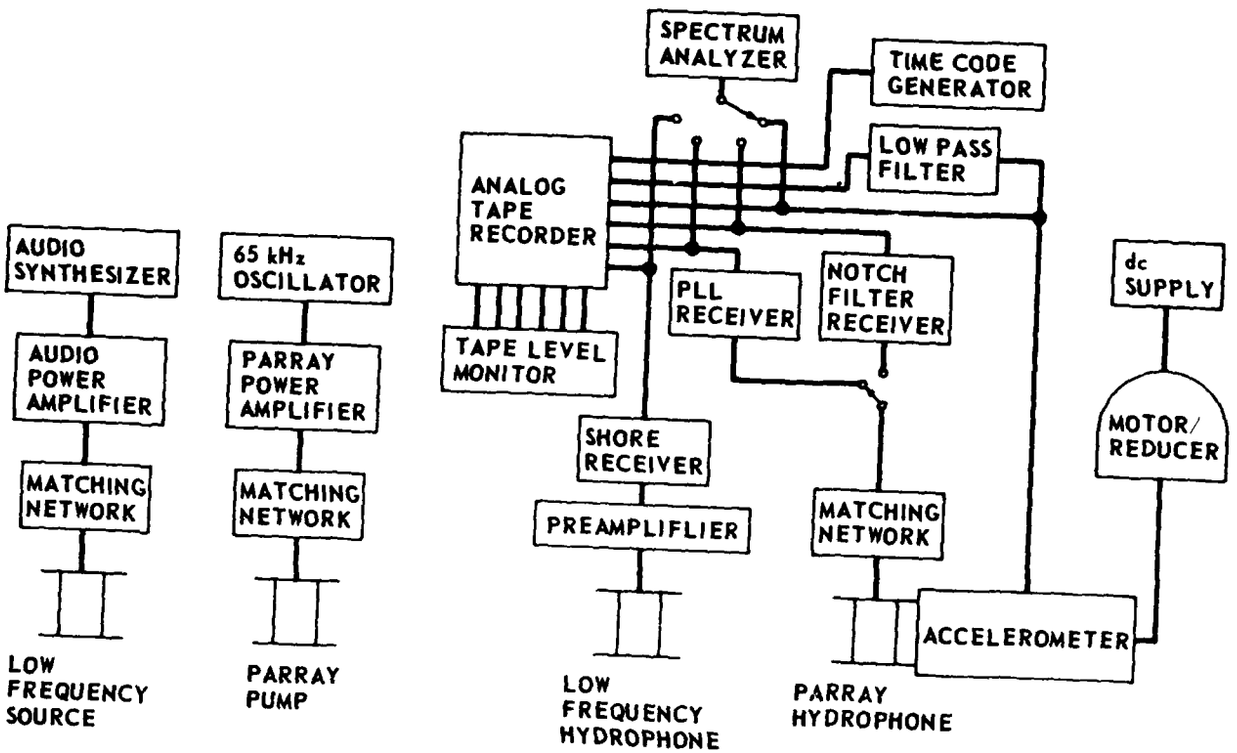

FIGURE 13
ACOUSTIC TEST INSTRUMENTATION

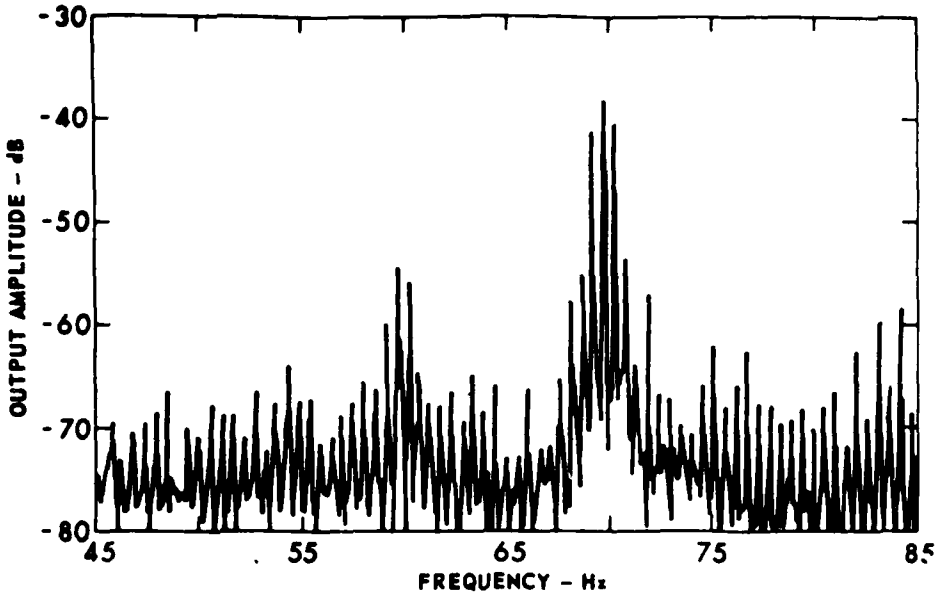

(a) NOTCH FILTER RECEIVER OUTPUT WITH VIBRATING HYDROPHONE

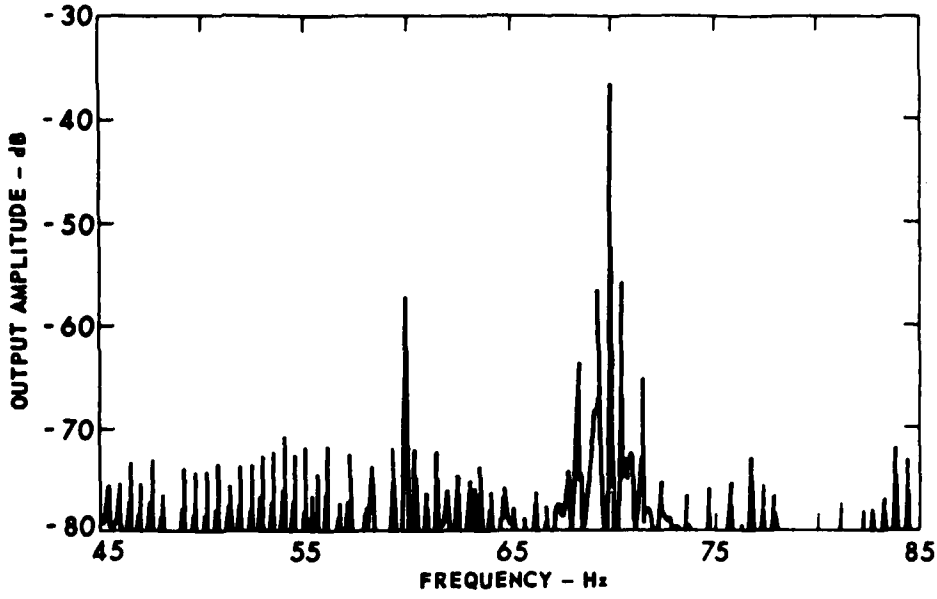

(b) PHASE-LOCKED LOOP RECEIVER OUTPUT WITH VIBRATING HYDROPHONE

FIGURE 14
COMPARISON OF DATA FROM PARRAY RECEIVERS
FOR VIBRATING HYDROPHONE
(d = 0.4 cm f_v = 0.53 Hz)

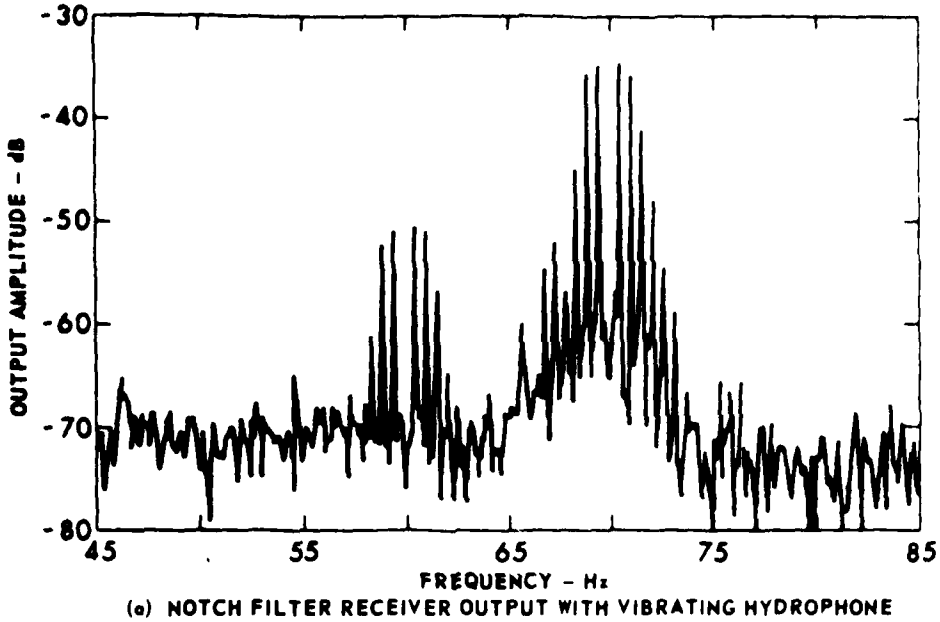

(a) NOTCH FILTER RECEIVER OUTPUT WITH VIBRATING HYDROPHONE

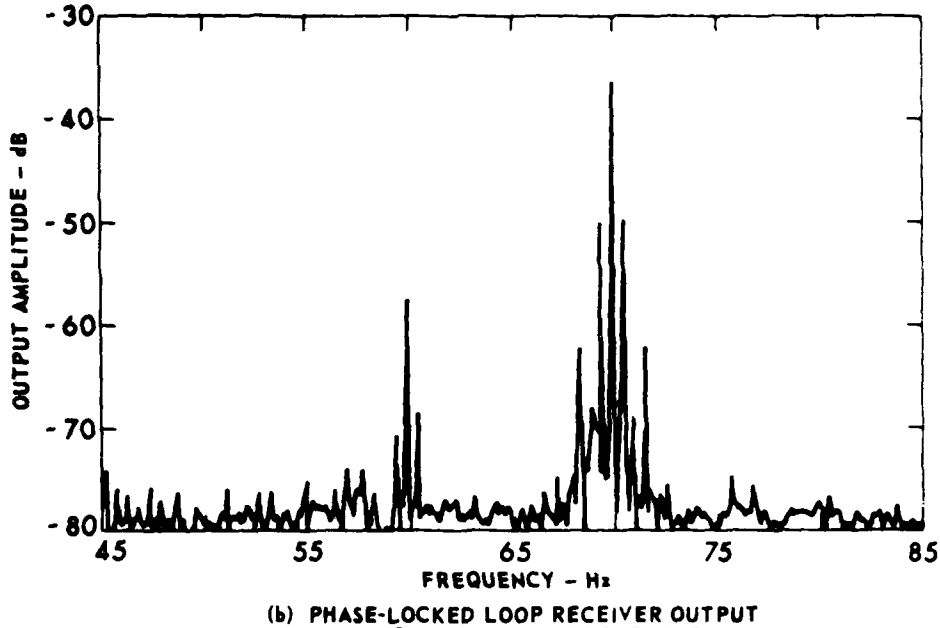

(b) PHASE-LOCKED LOOP RECEIVER OUTPUT WITH VIBRATING HYDROPHONE

FIGURE 15
COMPARISON OF DATA FROM PARRAY RECEIVERS
FOR VIBRATING HYDROPHONE
(d 0.85 cm f_v = 0.53 Hz)

the vibration induced sidebands around the acoustic tone at 70 Hz. Figure 14 shows a typical output spectrum for each receiver. In Fig. 15 the vibration modulation index is approximately 2.3, the value of the first null in the zero order Bessel function. This means that the 70 Hz signal is greatly attenuated due to the vibrational phase modulation. These data indicate that the PLL receiver significantly attenuates the level of the sidebands caused by vibration of the PARRAY hydrophone.

Figure 16 shows data compiled from a number of curves like those in Figs. 14 and 15. The curve in Fig. 16 displays level of intermodulation sidebands as a function of peak transducer displacement, for the PLL receiver and for a notch filter receiver. These data show that the PLL receiver reduced the level of the intermodulation sidebands approximately 15 to 20 dB relative to the notch filter receiver.

Although the PLL receiver produced a significant improvement over the notch filter receiver, PLL intermodulation performance with a PARRAY differed significantly from electrical measurements. The main cause of this difference is suspected to be amplitude modulation caused by transducer rotational motion. This motion caused the alignment of the narrow-beam hydrophone to change as a function of time, thus modulating the amplitude of the hydrophone output. This modulation produced low frequency sidebands around the spectral lines in much the same manner as the longitudinal vibration induced phase modulation. Amplitude modulation of the received signal was noted as a varying carrier amplitude, as well as asymmetrical low frequency intermodulation sidebands. This difference in level of the two first order intermodulation sidebands indicates that the modulation process was not purely phase modulation.

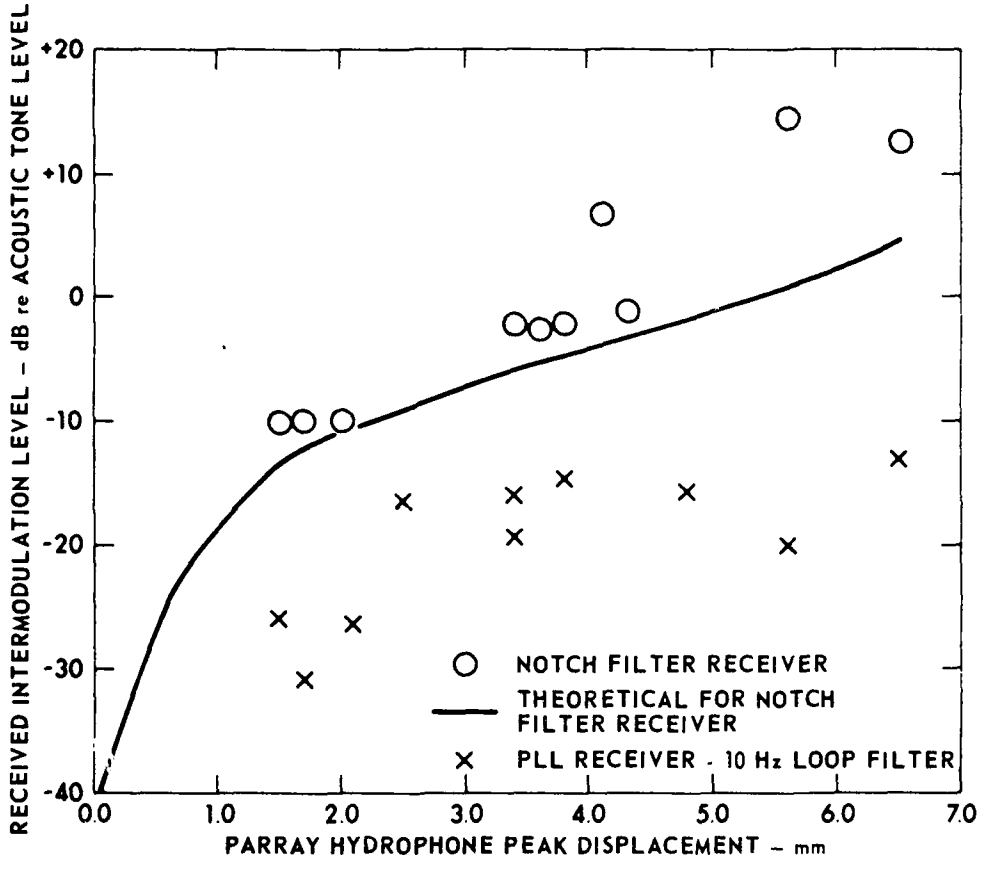

FIGURE 16
INTERMODULATION DATA FOR VIBRATING HYDROPHONE

In the next chapter a summary of the investigation of the PLL demodulator is given, some conclusions are made about its value for use with a PARRAY, and suggestions for future work are given.

CHAPTER IV

SUMMARY AND CONCLUSIONS

The purpose of the work described in this report was to evaluate the performance of a narrowband PLL receiver to determine its value in demodulating PARRAY signals. A number of tests were performed to measure the receiver performance and comparison was made between experimental intermodulation data and theoretical predictions derived in Chapter II.

Chapter II reviewed PARRAY operation and PLL fundamentals. The equations governing PLL operation were solved to allow prediction of intermodulation signal levels in the narrowband PLL demodulator. Intermodulation levels at the PLL output were separately derived for a PLL with a nonlinear VCO tuning characteristic and a sinusoidal phase detector characteristic.

Experimental work performed in evaluating a PLL receiver was described in Chapter III. Methods used to demodulate PARRAY signals were reviewed and a number of PLL receiver performance tests and their results were described. Very good agreement between theoretical predictions of frequency response and measured values was shown. Good receiver noise performance was demonstrated although further reduction in receiver noise is desirable. Reasonable agreement between predicted intermodulation levels and measured data was shown. The intermodulation tests were designed to measure performance of the PLL receiver with signals expected to be produced by a PARRAY undergoing transducer vibration. An acoustic test demonstrated good PLL receiver performance with a PARRAY undergoing vibration of its hydrophone. The latter test demonstrated the utility of a PLL demodulator in a PARRAY when transducer vibration is present.

Future work should address the problems of receiver noise and VCO linearity. Addition of an automatic gain control circuit to the receiver input would also be beneficial.

APPENDIX A

SPECTRUM OF TWO TONE PHASE MODULATION

The purpose of this appendix is to derive the magnitude of the important components of a signal that is phase modulated by the sum of two sinusoids. An example of this type of signal is the PARRAY hydrophone output when the PARRAY is receiving a single acoustic tone in the presence of high level, low frequency transducer vibration. The equations derived below are useful in predicting the output of a notch filter receiver with this type of input, and thus in evaluating the intermodulation sideband reduction achieved by a PLL receiver.

The specific type of signal to be examined is given by

$$s(t) = \cos[\omega_o t + \phi_i(t)] \quad , \tag{42}$$

where

$$\phi_i(t) = A_1 \sin\omega_1 t + A_2 \sin\omega_2(t) \quad , \tag{43}$$

A_1 = modulation index of the high level, low frequency modulation at frequency ω_1, and

A_2 = modulation index of the low level, high frequency modulation at frequency ω_2.

Equation (42) can be simplified by use of trigonometric identities and the relations

$$\cos(M \sin\omega t) = J_o(M) + 2J_2(M) \cos 2\omega t + 2J_4(M) \cos 4\omega t, \ldots, \tag{44}$$

$$\sin(M \sin\omega t) = 2J_1(M) \cos\omega t + 2J_3(M) \cos 3\omega t + \ldots, \tag{45}$$

where

$J_n(M)$ = nth order Bessel function of the first kind of argument M.

The resulting equation is:

$$s(t) = J_o(A_1)\, J_o(A_2)\, \cos\omega_o t$$
$$+ J_1(A_1)\, J_o(A_2)[\cos(\omega_o+\omega_1)t - \cos(\omega_o-\omega_1)t]$$
$$+ J_o(A_1)\, J_1(A_2)[\cos(\omega_o+\omega_2)t - \cos(\omega_o-\omega_2)t]$$
$$+ J_1(A_1)\, J_1(A_2)[\cos(\omega_o+\omega_2+\omega_1)t - \cos(\omega_o+\omega_2-\omega_1)t$$
$$+ \cos(\omega_o-\omega_2+\omega_1)t - \cos(\omega_o-\omega_2-\omega_1)t]$$
$$+ \text{higher order terms} \quad . \tag{46}$$

Equation (46) shows the frequency components of interest in s(t). The first three terms in the equation are the carrier, the low modulation frequency sidebands, and the higher modulation frequency sidebands. The fourth term contains the first order intermodulation components. This equation shows that the level of the intermodulation sidebands relative to the higher modulation frequency sidebands is the same as the level of the low modulation frequency sidebands relative to the carrier. This fact was used to experimentally determine the amplitude of the intermodulation tones since they were sometimes difficult to measure.

Equation (46) is somewhat difficult to use because of the nonlinear nature of the Bessel functions. However, for modulation indices A_1 and A_2 less than unity, the zeroth order Bessel function is approximately unity and the first order Bessel function is approximately

one-half its argument. Thus, Eq. (46) can be simplified for small modulation indices to give

$$s(t) = \sin\omega_o t + \frac{A_1}{2}\left[\cos(\omega_o+\omega_1)t - \cos(\omega_o-\omega_1)t\right]$$

$$+ \frac{A_2}{2}\left[\cos(\omega_o+\omega_2)t - \cos(\omega_o-\omega_2)t\right]$$

$$+ \frac{A_1A_2}{4}\left[\cos(\omega_o+\omega_2+\omega_1)t - \cos(\omega_o+\omega_2-\omega_1)t\right.$$

$$\left. + \cos(\dot{\omega}_o-\omega_2+\omega_1)t - \cos(\omega_o-\omega_2-\omega_1)t\right]$$

$$+ \text{higher order terms} \quad . \tag{47}$$

This equation was used to evaluate the results of the electronic measurements on the PLL receiver since low modulation indices were used. Larger modulation indices were encountered during the acoustic evaluation; therefore Eq. (46) was used in analysis of the acoustic data.

APPENDIX B

DETAILS OF PLL RECEIVER CIRCUIT

Details of the PLL receiver circuit used in the experimental work are presented here; a block diagram of this receiver was shown in Fig. 4.

Figure 17 is a schematic diagram of the receiver. An input transformer allows its use with high impedance PARRAY transducers or low impedance sources such as power amplifiers or oscillators.

Two crystal controlled oscillators can be selected to inject calibration signals at the phase detector input. These oscillators operate at 67.750 kHz and 65.275 kHz at levels of -110 dB re 1 Vrms and -120 dB re 1 Vrms, respectively. Accurate receiver calibration requires that the input device have a much lower impedance than that of the diode phase detector.

The phase detector consists of a double balanced Schottky diode mixer. This circuit consists of four Hewlett Packard 5082-2800 (1N5711) Schottky diodes and two center tapped input transformers. This type of phase detector provides better dynamic range than commercial double balanced mixers.

The phase detector output is low pass filtered to remove frequency components at the carrier frequency and its harmonics. The output of the filter is input to a low noise dc coupled operational amplifier (Fairchild μA739). This amplifier had better repeatability than circuits described in Refs. 21-22 as well as giving acceptable noise performance.

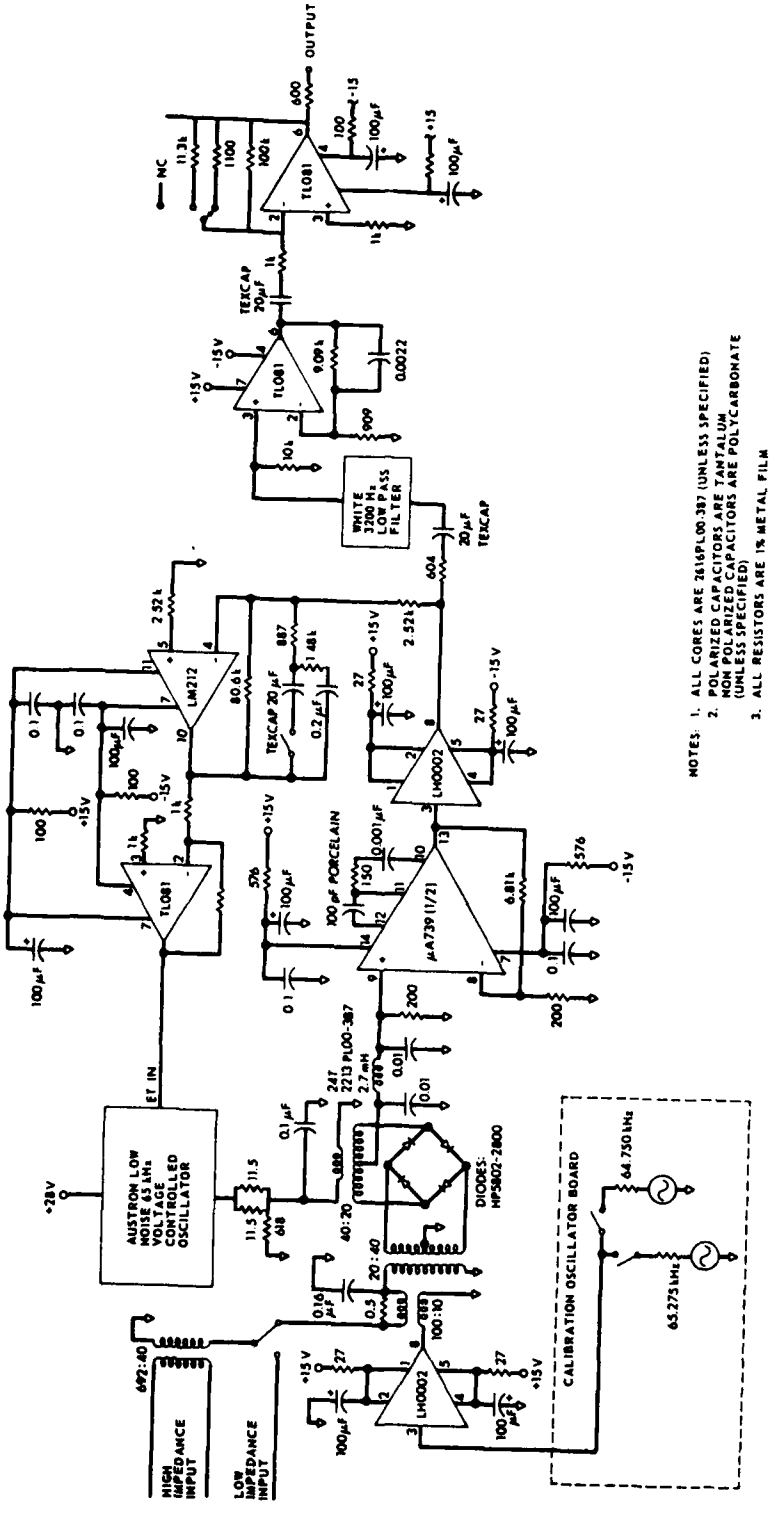

NOTES: 1. ALL CORES ARE 2616PL00-3B7 (UNLESS SPECIFIED)
2. POLARIZED CAPACITORS ARE TANTALUM
NON POLARIZED CAPACITORS ARE POLYCARBONATE
(UNLESS SPECIFIED)
3. ALL RESISTORS ARE 1% METAL FILM

FIGURE 17
PHASE-LOCKED LOOP RECEIVER

The gain of this circuit is 30 dB and its electronic noise is less than -165 dB re 1 V/$\sqrt{Hz}$ measured at 500 Hz with a source impedance of 200 Ω.

Because of the high output impedance of the μA739 amplifier, a National Semiconductor type LH0002 current amplifier is used to drive the next signal processing stage. The output of this amplifier must be filtered to reduce high frequency signals. The LH0002 drives the passive output filter as well as the active loop filter.

The output circuitry consists of a passive 3200 Hz low pass filter and two stages of amplification. The low pass filter is a commercial unit built by White Instruments, Austin, Texas. The specifications call for a 100 Ω input impedance, 10 kΩ output impedance, a voltage transfer function of -1 dB ±1 dB from 0 to 3200 Hz, and greater than 40 dB attenuation of frequencies greater than 4800 Hz. This filter passes the frequencies of interest while attenuating the carrier and its harmonics.

The output amplifier consists of two stages of Texas Instruments type TL081 amplifiers. The gain of the second output stage can be varied from 0 dB to 40 dB in 20 dB steps. This gain selection allows the receiver output to be set for optimum signal level into the tape recorder or spectrum analyzer.

Other components of the experimental PLL are the voltage controlled oscillator (VCO) and amplifiers which keep the VCO phase locked to the input signal. The loop low pass filter consists of an active single pole low pass filter with phase lead compensation and 30 dB of gain at dc. The low pass filter cutoff frequency is changed from 0.1 Hz to 10 Hz by switch selectable filter capacitors. Use of phase lead correction assures stability of the phase-locked loop in spite of extraneous

added phase shifts that may be present in the PLL. This phase lead correction was established to assure that the loop gain has only a 20 dB/decade slope (due to the integrating action of the VCO) at the frequency where the loop gain is unity. The phase lead zero of the filter response is set at the frequency where loop gain is +6 dB to assure stability despite gain variations. More information on PLL stability can be found in Ref. 27.

The output amplifier, which has 20 dB of voltage gain, amplifies the low pass filter output and drives the VCO input. The VCO used in this receiver is a very low noise unit manufactured by Austron, Inc., Austin, Texas. Specifications for this unit include single sideband phase noise in a 1 Hz band more than 165 dB below the carrier level for frequencies 100 Hz to 1 kHz from the carrier, and an electrical tuning range of ±5 Hz for ±15 V input.

The combined loop gain, including the phase detector and VCO gain, was approximately 80 dB. Measured phase detector gain was 0.398 V-sec/rad, VCO gain was 2.16 rad/V-sec. The total dc loop gain was 79 dB including the gain of all loop components. This value of loop gain was used in calculating theoretical loop frequency response and intermodulation performance for comparison with measured data.

BIBLIOGRAPHY

1. P. J. Westervelt, "Parametric acoustic array," J. Acoust. Soc. Am. 35, 535-537 (1963).

2. J. J. Truchard, "Parametric acoustic receiving array. I. Theory," J. Acoust. Soc. Am. 58, 1141-1145 (1975).

3. C. Richard Reeves, Tommy G. Goldsberry, and David F. Rohde, "Experiments with a Large Aperture Parametric Acoustic Receiving Array," Record of the International Conference on Acoustics, Speech, and Signal Processing, Washington, D.C., 2-4 April 1979. Also published in "PARRAY Technology Papers Presented at Scientific and Technical Meetings," Applied Research Laboratories Technical Report No. 79-4 (ARL-TR-79-4), Applied Research Laboratories, The University of Texas at Austin, 2 August 1979. AD A077726.

4. Tommy G. Goldsberry, "The PARRAY as an Acoustic Sensor," Applied Research Laboratories Technical Paper 79-42 (ARL-TP-79-42), Proceedings of the Conference on Underwater Applications of Nonlinear Acoustics, Institute of Acoustics, The University of Bath, Bath, England, 10-11 September 1979.

5. V. A. Zverev and A. I. Kalachev, "Modulation of sound by sound in the intersection of sound waves," Sov. Phys.-Acoust. 16, 204-208 (1970).

6. C. Richard Reeves, Tommy G. Goldsberry, David F. Rohde, and Voldi E. Maki, Jr., "Parametric acoustic receiving array response to transducer vibration," to be published in J. Acoust. Soc. Am., May 1980.

7. James J. Truchard, "Modulation Characteristics for Parametric Receiving Arrays," J. Phys. (Paris), Colloque C8, Supplement to N-11, 40, 140-145 (1979).

8. Paul W. Lewis and Wayne H. Weingarten, "A comparison of second, third and fourth order phase locked loops," IEEE Trans. Aerospace and Electronic Systems AE-3, 720-727 (1967).

9. R. C. Tausworthe, "Improvements in deep space tracking by use of third-order loops," Jet Propulsion Laboratory Quarterly Technical Review No. 1, Jet Propulsion Laboratory, Pasadena, CA, 1971, pp. 96-106.

10. F. M. Gardner, Phaselock Techniques, 2nd Ed. (John Wiley & Sons, New York, 1979), pp. 8-9.

11. Alain Blanchard, Phase-Locked Loops Application to Coherent Receiver Design, (John Wiley & Sons, New York, 1976), pp. 51-52.

12. William C. Lindsey and Robert C. Tausworthe, "A Bibliography of the Theory and Application of the Phase-Lock Principle," Jet Propulsion Laboratory Technical Report 32-1581, Jet Propulsion Laboratory, Pasadena, California, 1 April 1973.

13. Donald L. Schilling and Marc Smirlock, "Intermodulation distortion of a phase locked loop demodulator," IEEE Trans. Communication Technology COM-15, 222-228 (1967).

14. C. Melvil Thomas, "Distortion in the Phase-Locked Demodulator with Television and Multichannel Telephony," Proceedings National Electronics Conference XXIV, December 1968, 396-401.

15. Blanchard, op. cit., pp. 326-327.

16. Gardner, op. cit., pp. 168-170.

17 D. F. Rohde, T. G. Goldsberry, W. S. Olsen, and C. R. Reeves, "Band elimination processor for an experimental parametric acoustic receiving array," J. Acoust. Soc. Am. 66, 484-487 (1979).

18. T. G. Goldsberry, Personal communication.

19. C. Richard Reeves, "A Mixer-Receiver for the Parametric Acoustic Receiving Array," Applied Research Laboratories Technical Report No. 78-33 (ARL-TR-78-33), Applied Research Laboratories, The University of Texas at Austin, 18 September 1978.

20. Jacques Rutman, "Characterization of frequency stability: A transfer function approach and its application to measurements via filtering of phase noise," IEEE Trans. Instrumentation and Measurement IM-23, 40-48 (1974).

21. D. A. Howe, "Frequency Domain Stability Measurements: A Tutorial Introduction," NBS Tech. Note 679, National Bureau of Standards, Boulder, Colorado, March 1976.

22. Donald G. Meyer, "A test set for the accurate measurement of phase noise on high-quality signal sources," IEEE Trans. Instrumentation and Measurement IM-19, 215-227 (1970).

23. Jacques Rutman, "Characterization of phase frequency instabilities in precision frequency sources: Fifteen years of progress," Proc. IEEE 66, 1048-1075 (1978).

24. Jacques Rutman and Gerard Sauvage, "Measurement of frequency instability in time and frequency domains via filtering of phase noise," IEEE Trans. Instrumentation and Measurement IM-23, 515-518 (1978).

25. Charles L. Alley and Kenneth W. Atwood, Electronic Engineering, 3rd ed. (John Wiley & Sons, New York, 1973), 672-673, 692.

26. M. Ward Widener, "The development of high-efficiency narrow-band transducers and arrays," to be published in J. Acoust. Soc. Am., March 1980.

27. Blanchard, op. cit., pp. 60-76.

5 May 1980

DISTRIBUTION LIST FOR
ARL-TR-80-25
UNDER CONTRACT N00024-77-C-6200, Item 0011
UNCLASSIFIED

Copy No.

Commander
Naval Sea Systems Command
Department of the Navy
Washington, DC 20362

1 Attn: Mr. C. D. Smith, Code 06R/63R
2 Mr. D. E. Porter, Code 63R
3 CAPT R. H. Scales, PMS 402
4 Mr. D. L. Baird, Code 63X3
5 CDR D. F. Bolka, Code 63G
6 Mr. D. M. Early, Code 63D
7 Mr. John Neely, Code 63X3

Commander
Naval Electronic Systems Command
Department of the Navy
Washington, DC 20360

8 Attn: CAPT H. Cox, PME 124
9 Dr. J. A. Sinsky, Code 320A

Defense Advanced Research Projects Agency
1400 Wilson Boulevard
Arlington, VA 22209

10 Attn: CDR V. P. Simmons (TTO)
11 Dr. T. Kooij

12 Chief of Naval Material
Department of the Navy
Washington, DC 20360

Director
Naval Research Laboratory
Department of the Navy
Washington, DC 20375

13 Attn: Code 8150
14 Dr. M. Potosky, Code 8109
15 Dr. J. Jarzynski, Code 8131
16 Dr. R. D. Corsaro

Distribution List for ARL-TR-80-25 under Contract N00024-77-C-6200, Item 0011 (Cont'd)

Copy No.

Naval Research Laboratory
Underwater Sound Reference Division
P. O. Box 8337
Orlando, FL 32806
17 Attn: Dr. Lee Van Buren
18 Dr. Peter H. Rogers

Commanding Officer
Naval Ocean Systems Center
Department of the Navy
San Diego, CA 92152
19 Attn: Dr. H. Schenck, Code 71
20 Mr. M. Akers, Code 724
21 Dr. H. P. Bucker

Office of the Chief of Naval Operations
The Pentagon
Washington, DC 20350
22 Attn: CAPT Bruce Gilchrist, OP-95
23 CAPT J. R. Seesholtz, OP-95

Officer-in-Charge
New London Laboratory
Naval Underwater Systems Center
Department of the Navy
New London, CT 06320
24 Attn: M. B. Moffett, Code 313
25 W. L. Konrad

Chief of Naval Research
Department of the Navy
Arlington, VA 22217
26 Attn: Mr. R. F. Obrochta, Code 464
27 Dr. L. E. Hargrove, Code 421

Commander
Naval Ocean Research and Development Activity
NSTL Station, MS 39529
28 Attn: Dr. A. L. Anderson
29 Dr. S. W. Marshall

Commanding Officer
USCG Research and Development Center
Avery Point
Groton, CT 06340
30 Attn: CAPT M. Y. Suzich

Distribution List for ARL-TR-80-25 under Contract N00024-77-C-6200, Item 0011 (Cont'd)

Copy No.

31-43	Commanding Officer and Director Defense Technical Information Center Cameron Station, Building 5 5010 Duke Street Alexandria, VA 22314
	Battelle Columbus Laboratories 505 King Avenue Columbus, OH 43201
44	Attn: TACTEC
	Applied Research Laboratory The Pennsylvania State University State College, PA 16801
45	Attn: Dr. F. H. Fenlon
	Westinghouse Electric Corporation P. O. Box 1488, MS9R40 Annapolis, MD 21404
46	Attn: Mr. A. Nelkin
47	Dr. P. J. Welton
	Raytheon Company P. O. Box 360 Portsmouth, RI 02871
48	Attn: Mr. J. F. Bartram
49	Mr. E. P. Aurand 19 Hanapepe Place Honolulu, HI 96825
	Department of Engineering and Applied Science Yale University New Haven, CT 06520
50	Attn: Dr. P. M. Schultheiss
	RAMCOR, Inc. 800 Follin Lane Vienna, VA 22180
51	Attn: Mr. V. J. Lujetic
	Systems Planning Corporation 1500 Wilson Blvd., Suite 1500 Arlington, VA 22209
52	Attn: Mr. Jack Fagan

Distribution List for ARL-TR-80-25 under Contract N00024-77-C-6200, Item 0011 (Cont'd)

Copy No.

Bolt, Beranek, and Newman, Inc.
50 Moulton Street
Cambridge, MA 02138
53 Attn: Dr. J. E. Barger
54 Dr. F. J. Jackson

Marine Physical Laboratory of
The Scripps Institution of Oceanography
San Diego, CA 92152
55 Attn: Dr. William S. Hodgkiss

TRACOR, Inc.
6500 Tracor Lane
Austin, TX 78721
56 Attn: Mr. J. Dow

Radian Corporation
8500 Shoal Creek Blvd.
Austin, TX 78758
57 Attn: Mr. Jerry L. Bardin
58 Mr. Voldi E. Maki
59 Dr. C. Richard Reeves

60 Office of Naval Research
Resident Representative
Room 582, Federal Building
Austin, TX 78701

General Physics Corporation
10630 Little Patuxin Turnpike
Columbia, MD 21044
61 Attn: Dr. Frank Andrews

62 Physical Acoustics Division, ARL:UT

63 Garland R. Barnard, ARL:UT

64 David T. Blackstock, ARL:UT

65 Jimmy Byers, ARL:UT

66 C. Robert Culbertson, ARL:UT

67 Tommy G. Goldsberry, ARL:UT

68 John M. Huckabay, ARL:UT

Distribution List for ARL-TR-80-25 under Contract N00024-77-C-6200, Item 0011 (Cont'd)

Copy No.	
69	Robert A. Lamb, ARL:UT
70	Thomas G. Muir, ARL:UT
71	David F. Rohde, ARL:UT
72	J. Tom Vittek, ARL:UT
73	M. Ward Widener, ARL:UT
74	Reuben H. Wallace, ARL:UT
75	Library, ARL:UT
76-100	ARL:UT Reserve


DATE
ILMED
-8